POLITECNICO DI TORINO

Master's degree in aerospace engineering

Master's Degree Thesis

Design of a drone based injection system for pine and oak processionary treatment.

Supervisors

Prof. Matteo Davide Lorenzo DALLA VEDOVA

Prof. Paolo MAGGIORE

Prof. Edmondo MINISCI

Candidate

Filippo MANOLIO

DECEMBER 2023

Summary

The aim of this work is the preliminary design of a cost-effective, eco-friendly, and reliable injection system for the treatment of the pine and oak processionary moths. The system has been designed to be integrated with a commercial drone, namely the DJI m300 or DJI m350 drones. The proposed system includes a mobile arm enabling the precise injection of a liquid suspension containing dispersed fungal spores directly into the nests, thereby mitigating environmental contamination. The design approach considered the preferred use of commercially available components, where feasible. Computer-Aided Design (CAD) has been used for the realization of the components, coupled with structural analysis through Finite Element Method (FEM) software. Market-available components have been selected and included in the analyses. The work, carried out in collaboration with the University of Strathclyde and Ergatek s.r.l., is the initial phase of a longer term project to develop a drone based system able to recognise and treat the nests fully autonomously.

Acknowledgements

Table of Contents

List of Tables

List of Figures

Acronyms

PPM

Pine processionary moth

FEM

Finite element method

CAD

Computer-aided design

MTOW

Maximum take off weight

OEW

Operative empty weigth

UAV

Unmanned aerial veichle

UAS

Unmanned aircraft system

EASA

European aviation safety agency

PET

Polyethylene terephthalate

PETG

Polyethylene terephthalate glycol

PLA

Polylactic acid

PVC

Poly vinyl chloride

BTK

Bacillus Thuringiensis Kurstaki

BT

Bacillus thuringiensis

FPV

First-person view

RTK

Real-time kinematic

IP

Ingress protection

DC

Duty cycle

EU

European Union

DOF

Degrees of freedom

STS

Standard scenario

EVLOS

Enhanced Visual Line Of Sight

BVLOS

Beyond Visual Line Of Sight

WBS

    Work breakdown structure

WP

    Work packages

RPM

    Repetitions per minute

PLC

    Programmable Logic Controller

VFD

    Variable frequency drive

ISO

    International Organization for Standardization

NPSH

    Net Positive Suction Head

NPSHr

    Net Positive Suction Head required

EPDM

    Ethylene Propylene Diene Monomer

PPS

    Polyphenylene sulphide

PEEK

    Polyether ether ketone

Chapter 0

Processionary

0.1 Processionary moth

The processionary moth (scientific name Thaumetopoea pityocampa for the pine species, more in general Thaumetopoea processionea[1]) is an invasive insect, phytophagous and thermophilic, that mainly affects pines and oaks and represents a serious and destructive problem for the environment. The problem has become way more serious after its spread in the northern region of Europe, whereas it was initially prevalent mostly in Asia (Middle East), Africa and southern Europe.

0.2 Biological cycle

Its biological cycle gives life to a generation per year.

The adults of the species are moths with a short lifespan of only two days (difficult to distinguish from other species of moth). Between July and September they emerge from the soil where they may pupate if the level of infestation is very high. They copulate during the night hours and after that the female specimen lays between 70 and 300 eggs (1), most of the time at the end of August, on the sun-exposed branches of the host plant. [2]

The eggs hatch after 30-45 days, and the larvae remain sheltered during the coldest months of the year up on the tree until the next spring (April/May), when the plants begin to vegetate, providing them nourishment. The larvae, taking their resources from the leaves of the tree, damage it and the ecosystem.

They also are characterised by nocturnal behavior, and move together one in a row to another, while at sunset they return to their nest.

These caterpillars, only 2 mm long when they emerge, tend to remain in the trees until they grow older and reach 1 cm length developing the hairs, becoming a problem for humans and animals.

Figure 1: Processionary's eggs.[3]

The urticating hairs (shown in figure 2) develop from the dorsal side of the insect and are used by it as an arm of defence against predators. The length of the hair is approximately 200μm, while the diameter is about 5 μm.

At the end of the caterpillar phase, they can reach 2 cm in length.

After some time, usually in the months of June and July, the larvae form a cocoon in the nest (or in the soil as said before) which, after 30 days, gives birth to new adults.

Two curiosities are important to understand the danger of this pest: the first one is that some larvae can remain undisclosed, dormant, for two or three years, giving a dangerous and casual distribution of the insect over time. The second one is that when there is a severe infestation, the larval phase can be carried out in the ground.

0.3   Nest

The nest is a white silky cluster that can reach the size of a football. It is built between September and October from the remaining webs of the larvae's activity and serious.

The tissue of the nest is very elastic and stratified, with a thickness of a few millimetres. They are usually found in early summer, due to the biological activity of the processionary.

A single host tree can contain multiple nests at any height from the ground. They are typically dome or teardrop shaped for the oak processionary.

When they are fresh they appear white, then they turn brown and so they are more difficult to spot. After a life cycle, the nest is no longer used by other generations of processionary moths.
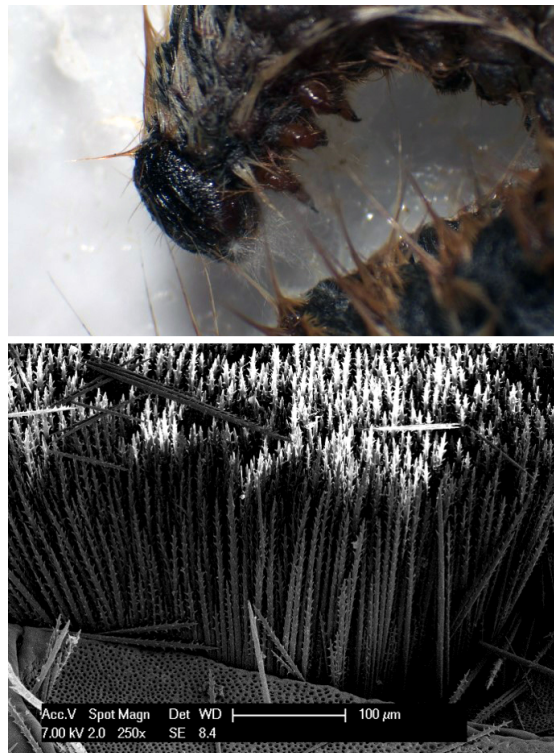
Figure 2: Processionary's hairs. [2]

Sometimes, during occasional hot days in March, the larvae may exit from the original nest to feed, and it is possible that they may built others new smaller nests.[2]

0.4 Damages and risks

The caterpillars present large and urticating hairs containing a toxin called "Thaumatopina", which can cause serious harm to the respiratory system of small animals, such as dogs (figure 4), and irritation to the human skin (figure 3), skin rashes and breathing difficulties. In some rare cases the hairs may trigger an allergic reaction.

In addition, the caterpillar nests, located in the branches and foliage of pine and oak trees, may contain some rests of the urticant hairs, so the removal has to be carried out carefully by experts with the proper equipment and chemical solutions, as illustrated in the picture 5.

The hairs may also be blown about in the wind, so even being near infested trees can be dangerous.

For plants the risks are linked to a reduced productivity of trees due to defoliation:

Figure 3: Skin reaction to pine processionary. [4]

Figure 4: Dog tongue reaction to pine processionary. [5]

Figure 5: Operator removes processionary nest. [6]

this factor can lead to a weakness of the trees, making them more susceptible to other diseases.

Even though moths can fly between 1.5 and 1.7 kilometres in their lifetime, control over imported products such as trees and soil is not enough, so the pest could spread over many countries with the process of globalization.

To resume the risks:

- allergic skin reactions;

- mucosal allergic reactions (with possible anaphylactic shock);

- damage to animals' mouth that can cause tongue necrosis;

- defoliation of the pine;

- fire danger in defoliated trees areas.

Chapter 1

Project

1.1 Project aim

This project aims to develop a low-cost and environmentally friendly injection system to prevent and fight the diffusion of the pine and oak processionary moth. That plague lately has resulted to be a critical environmental issue, affecting flora and fauna.

The goal is to front the moat problem cutting its life cycle through precision injections in its nest, killing the insect during its caterpillar phase, when is more vulnerable because not yet fully developed and strong. By intervening before it can reach the ground during the hottest season of the year, the caterpillar cannot built its cocoon under the ground, and it cannot transform itself in a butterfly. In the spring season intervention against the caterpillar is too late, it is necessary to face the problem during the autumn/winter season. For this reason and to prevent the falling of the nest due to its own weight, the nests are treated in their early stages.

The chosen approach to combat this insect is the use of a drone, this means that all the limits of the manual treatments in reaching difficult areas can be overcome. In the initial phase it will be remotely controlled by an operator, then it will be adapted and upgraded with AI for autonomous flight capabilities and software for the automatic recognition of nests and the implementation of the necessary routine to perform for the injection (including the approaching phase, contact with the nest and departure).

The drone that has been chosen for this application must be a drone with important cargo capabilities, so it should have an available payload that can provide the project engineer a large space of manoeuvre to choose the right components, able to perform the job.

Additionally, this drone has to be equipped with sensors and cameras adequate for the second part of the project (autonomous flight and injection), and the

resistance of the drone to the operating environment has to be taken in account, because impact between the propellers and little leaf of the trees may occur.

The precision injection given by this method can ensure a low-impact operation as the fluid is released inside the nest and there is no dispersion in the surrounding environment if compared to the actual methods.

The technology proposed in this field can bring very important advantages:

- it is safer for other animal species and plants because it is not based on spraying or misting methods over an entire area using helicopters and light aircraft, which can lead to the dispersion of the product, but is localised and extremely accurate;

- for the previous point, it does not require a quarantine of the treated area;

- it does not harm the plant because there is no need to cut the branches;

- is safer for the operator who can lead the intervention at a safe distance from dangers;

- the covered area is much bigger and it is possible to reach difficult points;

- it is significantly more economic.

1.2   Injected liquid

The injected liquid is a water-like fluid containing a dispersion of fungi spores. Currently, the dimensions of these spores are unknown, so is assumed that they will not be a problem for the diameter of the needle used.

However has to be taken in account (for future design, once the liquid characteristics will be given) the possibility of needle obstruction due to the aggregation of different spores forming clusters.

For the other considerations we assume the same density and viscosity as water.

1.3   Project phase

The thesis begins from ground zero, so the first phase of the project is the 0 phase, in which there are a lot of opportunities to set different architectures to address the problem and fulfil the requests of the client.

In this first phase it is usually good practice to perform a feasibility study, stakeholders research and analysis, study of the possible architecture, solutions and so on.

The priority is to design the mission itself and the elements needed for the program implementation: the final result of this work is to understand how to design almost from zero level and full decision-making power a mission with the goal required from the ''Ergatek'' company.

This is a multidisciplinary process that should involve many roles and stages, but the work will be condesed so that it will be possible to go deeper in the project in one aspect and test the product on software resources.

For this reason the focus is principally on the CAD realisation of the structure, structural testing, research on materials, components and the definition of some other crucial initial parts, while the electrical and control aspects will be left to further phases.

The tools used to develop the work are basically some codes implemented on Matlab software and CAD tools for the realisation of assembly and components analysis with the finite element method (FEM), used to verify if the structures can withstand all the loads developed during the exercise of its functions.

CAD softwares used include Autocad Inventor, Autocad Inventor Nastran and Ansys: this approach is useful to compare different results in software that may approximate in different ways materials properties.

To summarise, is possible to evaluate different parts of this project, but the focus will be on the design phase and then the result of the analysis will be handed to others engineers able to carry on other phases:

1. design

2. production

3. verification

4. training

5. operations

6. results analysis

The design phase aims to understand the objective of the mission, who is interested in it (stakeholder) and how it can be possible to design it.

Then the production involves acquiring components buying them from the market, or at least the materials and tools to construct them, build the infrastructure and finish with the assembly of the systems.

Verification phase ensures that everything is working as planned and tests the systems.

The training phase in this project will not be so important, because the only human resource during operations is the drone pilot, who already is in possession of the UE flight licence from EASA needed for this kind of drone and operation.

The drone bought by the company falls, for its use, in the specific category, so the licence required is the EASA STS [7].

For the EASA certification, the pilot will be professionally and widely trained. To obtain certifications related to EVLOS and BVLOS operations, he is required to complete a training course which includes 24 hours of theoretical lessons about security, aeronautical regulation, navigation, human factors and more. Additionaly, there are 8 hours of practical training in different scenarios: cargo, night flights, flights over populated areas and crowds, object drop, particularly relevant for our project, operations on mountains [8].

The remaining formation process is about the nests, the processionary and the implementation of the system to use, that should be considered as it modifies slightly the manoeuvrability of the drone but considerably its dimensions.

Only in a second phase the training will also include a part for the control of data associated with remote and autonomous operations and coordination with other drones capable of locating and communicating the position of the nests.

The operations phase will be executed as explained later in the chapters. However, for the first prototype, a visual light of sight (VLOS) procedure will be used, involving human coordination and monitoring: during these procedures an operator will be always present and capable of monitoring the drone and the entire injection process.

At the conclusion of the realisation of this first drone version, the results will be analysed and the system will be improved for the implementation of the autonomous version of the drone.

The system design of the product starts with a requirements definition and a technical solution definition.

The iterative process behind all this will guide the engineers through functional analysis, synthesis, optimization, definition, design, test and evaluation, with particular interest in the reliability, maintainability, producibility and structural integrity aspects.

Last but not least, is important the economic factor, to achiev a cost-effective solution within the budget that the stakeholder imposed.

Program management is essential to satisfy customer performance needs within the agreed conditions of time and cost. To proceed in an organised and structured way, it is good practice to clearly define objectives, divide the program into manageable sub-elements and set also a quality standard.

Some tools used are

- the functions tree (1.1), which is the breakdown of the system performance into functions further divided into sub-functions, and is an helpful hand during the mission definition phase;

- the product tree (1.2), which is similar to the functions tree and linked to it

but it breakdown the project in hardware and software elements.
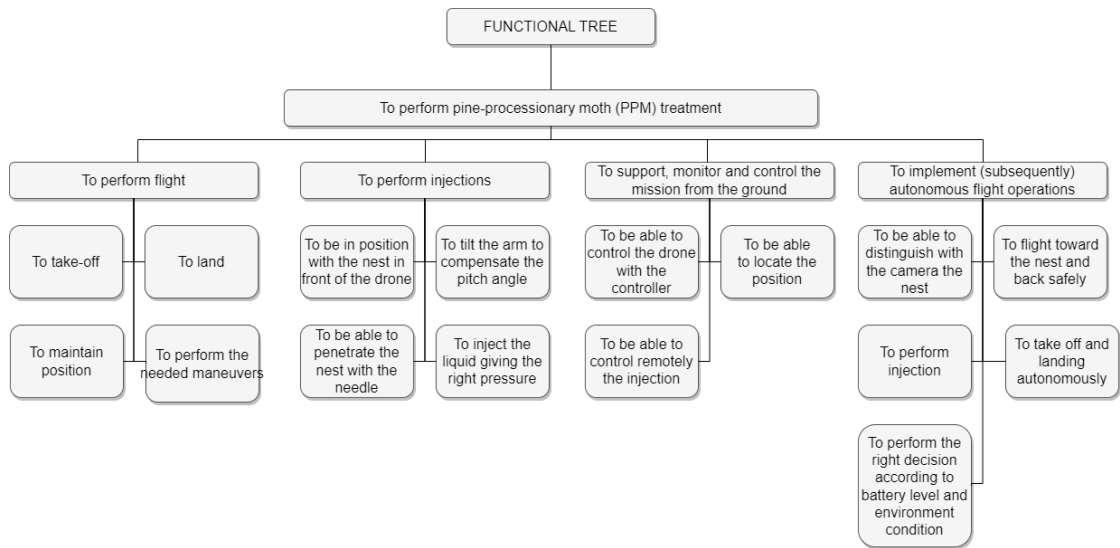
Figure 1.1: Functions tree
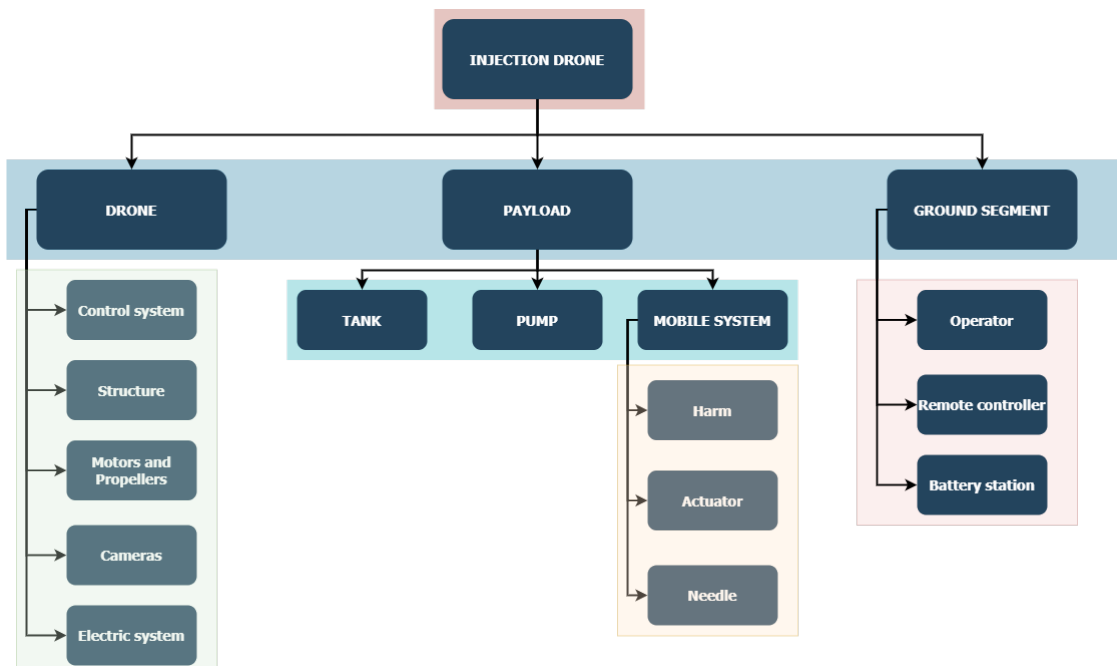
Figure 1.2: Product tree

1.4   New frontiers in drone use

Nowadays, the use of technology is implemented in every field, even the ancient ones: constructions, oil and gas, electricity and public security. In particular, the development of drones which are now more affordable, easier to use and more reliable, give to everyone the opportunity to invest in and change their type of production, improving it.

Another important aspect to consider is the one that guided this thesis project, the fact that payloads of different purposes can be created and implemented on commercial drones to accomplish different tasks, and they are easy to adapt to existing structures and power outlets with the right adjustments.

In conclusion, more companies are equipping their workers with these powerful instruments, reducing the risks by involving human contact with the dangers only in the necessary and unavoidable cases. However it is not the only important step in the digitalization of jobs: having drones with specific equipment and payloads gives the opportunity to collect data like photos, thermal images, infrared data (and so on) which can be processed later in the office or even in real time.

We can see some examples of different applications

- inspections through cameras and other optical sensors;

- photogrammetry, 3D mapping and surveying;

- farming (increasing agricultural production, inspection of plants, agricultural treatments. . .);

- defence;

- constructions;

- search and rescue thanks to thermal sensors;

- media and cinema thanks to the powerful cameras with high quality resolution.

[9]

1.5   Current methods for PPM's fight

In Italy, the fight against this type of moth is mandatory and declared by a law enacted on October 30, 2007. This undersores how serious the problem is.

The current methods to prevent the spread of the processionary moth involve human operations with specialised personnel to physically remove the caterpillar nest or spraying them with some liquids to impregnate them, exposing to risks the

staff involved and other animals as the nest can contain some urticating hairs that may be blown by the wind. The figure 1.3 is a clear example.

In each case a specialised company should carry out the necessary operations using specific products certified by the ministry.

Figure 1.3: Procedure to remove processionary nest [6].

The official guide lines on the use of phytosanitary products in the fight against the processionary moth, from 1998, establish the use of "bacillus thuringiensis var. kurstaki" to be sprayed on the tops of the trees, and that is effective only during the larval stage, between August and September, when the larva is not closed yet in the nest [2].

Here is a list of the options used to control this pest, later on more in-depth considerations on their economic and environmental impact will be made.

- The first method is the physical removal of the nest and subsequent destruction of it. This requires reaching the nest itself via ladders or platforms, depending on the height of the nest, by a specially equipped operator dressed in protective

clothing. Moreover, this method is effective only during the winter period, when the processionary moth larvae are still inside the nest.

- The second method is the one already mentioned. It is the most widespread and consists of spraying the environment with a bacterium capable of affecting the processionary moth's nervous system.

  The biggest drawback, and also the most obvious, is that the treatment is not always localised as it can be carried out on a large scale by helicopter spraying.

  Even if a knapsack sprayer is used, the substance would still be spread in the environment because the treatment is outside the nest. It would also involve the use of an operator on foot with the same complications as the previous point regarding reaching the nest and transporting the equipment.

- The preventive method is the use of pheromones that can, during the summer months of moth mating, confuse the male specimen and thus prevent it from meeting the female specimen.

- Glue traps that block the path of caterpillars on tree trunks.

- Endotherapy method, which consists of injecting insecticides directly into the plant so that they spread to its leaves. By doing so, the larvae feeding on the plant will be poisoned.

  According to the companies using this treatment, it does not harm the tree and, as it is adopted in the autumn just after the processionary moth eggs have hatched, the larvae have not yet had a chance to develop their urticating hairs and therefore there is no dispersion of them into the environment.

- Use of natural enemies of the insect such as the great tit, the common tit, the common chaffinch, the common blackbird and the common starling [10].

In the case of the most common treatment, with the bacterium Bacillus thuringensis, the product has a deficiency time (i.e. the time between treatment and harvesting of possibly contaminated fruit and vegetables) of 3 days [11].

1.6   Others works

It is important to mention that this project is not the first in this field. Two other companies have worked on this idea.

The difference between their work and this one is the implementation of the capability to moving the arm for controlling the injection, adapting the inclination of the arm to the pitch of the drone approaching the target.

This aspect is particularly relevant to ensure the right inclination of the part involved in the penetration, typically a needle, and also ensure the maximum horizontal force that the drone can give.

The first company is Fitobiotech s.r.l.[2], an innovative startup founded in 2017

Figure 1.4: Fitobiotech drone [2].

at the scientific and technological center of ComoNeXT, in collaboration with the Department of Biotechnology of the University of Insubria (which has the goal of creating robotic systems like drones to fight pests in specific situations) by Mattia Romani, an Italian architect.

The drone (1.4) with its arm was developed to move inside insidious and tree-covered areas where humans might struggle to reach nests.

The first step of this group is to localise the nests through photographic surveys and then proceed with the injection thanks to the equipped drone.

The product injected inside the nest nourishes itself of biological components leaving a dry nest that after some months degrades.

The other important group is Pitostinger [12], that in the beginning was focused on the processionary plague, but now they developed the drone so it can also fight other pests such as tiger mosquito and black fly.

The Spanish team, in collaboration with ESA business incubation centre, uses a static injection arm that is fixed to the bottom of a 4, 6 or 8 propelled drone (1.5) (different prototypes have been developed since 2019), and as they declare: « Our drone evolves day by day, improving its navigation and artificial vision system and also to detect that nest automatically (artificial vision) through its cameras and different sensors and in this way carry out the application autonomously.»[13].

With the use of high-tech drones, equipped with cameras, sensors, anti-collision

Figure 1.5: Fitostinger drone [13].

and air traffic detection systems, all the above abilities can be implemented.

In the field of pests control, they also developed "FitoVelu" (6 engines): this drone is dedicated to combact the Asian wasp (Velutina). The interesting upgrade on this drone is the telescopic pole, able to reach more distant nests.

Then it is important to mention other two important works of the group in the agricultural field: Phytoweed and Phytoagro.

Both drones are able to reach difficult areas (in the case of Phytoweed also vertical walls and side of buildings) to apply herbicides by diffusing the liquid with specific nozzles. The second one, Phytoagro, allows a wide variety of treatments [13].

Chapter 2

Drone

2.1 Drone technology

Unmanned aerial vehicles (UAV), also called drones, are identified as remotely controlled (or autonomous) vehicles without a pilot onboard, developed during the twentieth century for military purposes.

They are part of what is called unmanned aircraft system (UAS), which includes a system of communication with the drone and a pilot on the ground (or a controller if the drone is autonomous) to direct the flight [14].

The drones considered in this study are not designed for military applications, on the contrary they are developed to enhance industrial operations, mostly in surveillance, agricultural operations and even research and rescue operations. In the specific they are called remotely piloted aircraft systems (RPASs).

The technology involved in this study is integrated most of the time with first-person video and technological advanced cameras which contribute to the accomplishment of the assigned task.

Starting from the basic concepts, a drone can be a fixed wing aircraft or a rotary wing aircraft.

Fixed wing technology has some advantages such as higher speed and flight autonomy, due to the portance created by the wing's surface and the fuselage. On the other hand, they need space for takeoff and landing, while a multi-rotor drone is provided with more control, can flight in hovering mode (maintain a stationary position, very useful for taking good images, operate visual inspection and accomplish some delicate operations which require steady position or very slow movements) and it can takeoff and landing in small spaces.

The last solution is the single rotor (helicopter) drone, with a larger propeller: this provide a bigger lift force with less rotor spin, increasing the efficiency (there are obviously limitations to the length of the rotor blade). The number of propellers

is also determined by the lift force needed, related to the payload weight which the drone has to carry.

For this reason most of the drones used for agricultural applications, involved in pesticide distribution on cultivated fields, which have to carry heavy loads like the distribution system, liquid nebulization components and a tank that most of the time has a 10 litres capacity, have between 6 and 8 propellers.

The most common drones in the market are multirotor devices, able to produce lift thanks to the rotation of propellers that can spin at different speeds.

This aspect is crucial for creating momentum able to tilt the drone in pitch and roll and to create the yaw momentum as well.

To analyse the mechanics behind a multirotor drone, it is possible to resume here some architectures and features of the most common ones.

- the electric motors with the propellers for the thrust and momentum creation;

- the main structure which has the duty to connect all together providing structural resistance and at the same time a lightweight design;

- the power source, whether batteries or motor with fuel. In each case it represent the heaviest part of the drone. Usually lithium polymer batteries are used due to their high power density;

- all the electronics inside to coordinate, monitor and communicate with ground or remote controllers.

Thanks to the modern innovation in the manufactoring processes, the base structure is realised most of the time in plastic and composite materials, reducing the weight allowing increased payload capacity. Essentially it comprises a base with many arms as the number of propellers present on the drone.

This work will focus on the most diffuse architecture: the quadcopter.

The functioning is similar across all architecture but will be discussed this configuration because it is the one used by the drone given by the stakeholder and is easy to explain compared to others.

Considering a fixed-pitch rotor, there are 6 controllable degrees of freedom using. To allow proper operation and momentum balance, two rotors rotate anti-clockwise and two rotate in the opposite direction coupled on the diagonals.

When the revolutions of the rotors are the same, the pairs are balanced. Therefore, to generate a rotational torque around one axis, it is sufficient to upset this balance.

For roll and pitch you increase the power of one rotor and decrease that of the opposite rotor, for yaw you increase the torque on the motors on one diagonal and reduce that on the diagonal of the other two motors by the same amount.

16

More complex manoeuvres are a combination of the manoeuvres just described and are implemented with mathematical models (twelve equations) using Euler angles, rotation matrices and equations describing the coupled dynamics of the motions [15].

Operation		UAS			UAS Operator	Remote pilot	
Subcategory	Operating Area	Class	Mass/KE/Speed	Operating Date limitations	Registration	Min Age (solo flight)	Competency
All	- Max height 120m/400ft (see UAS.OPEN.010 [3] & [4] for specific obstacle and sailplane limits) - No dropping of articles - No carriage of dangerous goods					If directly supervising another remote pilot - 16	
A1	Fly over uninvolved people, but not over crowds	Privately built	<250g 'flying weight' and <19m/s	Nil	Only if 'camera' equipped (but not toys)	Nil	Read user manual
		Legacy (placed on market before 1 Jan 23)	<250g 'flying weight'				
		C0 (toy)	<250g MTOM and ≤19m/s				
		C0 (not a toy)					
	No intentional flight over uninvolved persons	C1	<900g MTOM or <80 J	Nil	Yes	UK – 13 EU – 16 (unless reduced in State)	• User manual • Online training • Online (foundation) test • A2 CofC Theoretical test
		A1 Transitional (Article 22)	<500g 'flying weight'	Not after 31 Dec 22			
A2	No closer than 30m horizontally from uninvolved persons (5m in 'low speed' mode)	C2 (can also be used in A3)	<4kg MTOM	Nil	Yes	UK – 13 EU – 16 (unless reduced in State)	- User manual - Online training - Online (foundation) test - Self-practical training - A2 CofC Theoretical test
	No closer than 50m horizontally from uninvolved persons	A2 Transitional (Article 22)	<2kg 'flying weight'	Not after 31 Dec 22			
A3	- No uninvolved people present within the area of flight - No flight within 150m horizontally of residential, commercial, industrial or recreational areas	C3	<25kg MTOM	Nil	Yes	UK – 13 EU – 16 unless reduced in State	- User manual - Online training - Online (foundation) test
		C4					
		Privately built	<25kg 'flying weight'				
		Legacy (placed on market before 1 Jan 23					
		A3 transitional (Article 22)	>2kg to <25kg 'flying weight'	Not after 31 Dec 22			

Figure 2.1: EASA open categories tabel.

Drones can be classified according to many aspects such as weight, engine type, autonomy, maximum ceiling altitude... [16],[17],[18]

For the European Union, EASA established the classification of drones, dividing the different classes on the base of a risk factor and, for the new regulation, is no longer requested a distinction between professional and recreational use.

According to the European regulation there are three main categories: open, specific and certified.

The open category is resumed in the table 2.1 and is further organised into three subcategories (A1, A2 and A3) within which drones from class C0 to class C4 can operate.

As we can see the A classes are defined by the weight and, consequently, by the distance of the operation from other people not involved.

The A1 class is for drones and operations that can be flown over people, A2 is for the ones near the people but not closer than 30 metres and A3 is for drones not allowed to fly next to residential and frequented areas (they must keep a distance of at least 150m).

From 31th December 2020 to 31th December 2023 drones which weigh is between 500 grams and 2 kilograms without a CE mark are classified as open limited category. From the first of January 2024 they will fall under the A3 category.

For those with a CE mark, the division is the following one:

- C0 for a weight under 250g;

- C1 for a weight under 900g;

- C2 for a weight under 4kg;

- C3 for a weight under 25kg.

The other two categories which may be useful to understand to set the differences and limits that this project has to maintain are written below.

The Specific category (in which the drones are operated when they are outside the operational limitations of the open category) regulated by the 5th article of Reg(UE) 2019/947, is applied to a medium risk level and requires the declaration from the UAS operator or operational authorization from ENAC [19].

Some examples of operations to be included in this category are:

- Beyond visual line of sight activity (BVLOS) and extended visual line of sight (EVLOS);

- MTOW over 25 kg;

- Flight altitude over 120 m;

- Dropping material;

- Drones with a MTOW over 4 kg or without class identification that operate in an urban environment.

Before starting a flight in the mentioned situations, the drone operator must obtain an authorization from the national aviation authority of the state of registration, unless the operation is conducted under an European standard scenario. Also, if the area in which the operation is conducted is covered by geographical zone, a flight authorization by the institution in charge of this zone is mandatory.

This applies to the open category as well.

Is usefull explain more in-depth the BVLOS and EVLOS situations as the drones operation that will be performed could be of this type: these two conditions are defined critical operations also because it is not feasible to apply collision avoidance manoeuvres in visual line of sight.

The EVLOS includes other operators such as an observer with binoculars or secondary pilots able to take control of the drone in case the principal pilot loses sight.

The BVLOS instead involves no visual contact between the pilot and the remotely controlled drone but relies on alternative methods to keep contact on the situation (FPV first person view for example).

The certified category, instead, is created for the highest risk operations, so the ones involving people as payload.

Is easy to understand that the approach and the normative is similar to the one applied to manned and civil aviation. Consequently, this type of drone will need to be certified and, eventually, the remote pilot will need a pilot's license.

An existing example of drones falling into this category are the ones conducting operations that carry cargo in urban areas following pre-defined routes in airspace where U-space services are provided [20].

All the operations in certified category are here resumed:

- Air taxi and in general UAS used to transport people;

- UAV with a dimension above 3 metres;

- Transport of dangerous goods;

- UAV flying in condition with ground risk class.

The application implemented is very similar to those in the agricultural field, in which a drone is equipped with irrigation system with nozzles to diffuse agricultural drugs in mainly two kinds of situations: large areas to treat or heroic agriculture.

Both these situations are beneficial in terms of time and economy, whit UAVs being controlled and automated over some areas.

The system is composed of the same components: tank, pumps (often diaphragm ones), valves, regulators and nozzles.

The difference is not so much in the system components but in the drone on which the system is mounted. For the kind of application that they have to satisfy, the dimension of the tank in such drones is larger, implying a bigger load and weight. Consequently the drone will be bigger in size and power, to be able to lift more weight and accomodate higher payload capacity.

2.2   DJI m300

The DJI Matrice 300 drone, as stated by DJI, is an industrial drone with advanced AI functionality and a large flight time of 55 minutes [21].

Thanks to its technology, it is able to offer great performance and is therefore used in various fields for inspection, research and mapping.

It has an IP45 rating, which means it is protected against the ingress of solid objects larger than 1 mm in diameter and protected against water jets pumped in from any direction [22].

Thanks to the integrated 1080p camera and transmission system, high-definition video can be achieved. This eliminates the need for an additional camera in our system because the integrated one is sufficient for the purpose of the project. This is certainly an advantage in terms of both weight and configuration.

Moreover the drone has an high stability and a good resistence to the wind (up to 12 m/s to the wind). This aspect make it appropriate to perform precise injection aiming to the nest even if it is limited in dimensions.

An aspect not to be underestimated is its ability to carry three payloads at the same time, as depicted in the picture 2.2. The position of the payloads is also advanced with respect to the centre of gravity of the drone itself, but the drone is easily able to compensate for the shift automatically.

This is reassuring for the payload of this study which, by its nature, is very forward leaning. Certainly some adjustments on the control system will be necessary, but this is something that will be considered later.

Figure 2.2: DJI m300 payload configuration [21].

Some of the main features to understand the performances and capabilities of the drone are resumed in the table 2.1.

Dimensions	Unfolded, prop excluded, 810×670×430 mm Folded, prop included, 430×420×430 mm
Weight	3.6kg (without battery) 6,3 kg (with two TB60 batteries)
Payload capacity	2.7kg
1 gimbal damper's max payload	930g
MTOW	9kg
Max hovering accuracy	Vertical: 0.1m RTK or vision system enabled; Horizontal:0.1m RTK enabled
RTK positioning accuracy	1cm+1ppm (horizontal) 1.5cm+1ppm (vertical)
Max angular velocity	pitch 300°/s yaw 100°/s
max pitch angle	30°
Max speed	S mode: 23m/s P mode: 17m/s
Max wind resistance	12m/s
Max flight time	55min
Ingress protection rating	IP45
Operating temperature	-20°C to 50°C

Table 2.1: Specifications DJI m300.

2.3 DJI m350

The DJI Matrice 350 drone is very similar to the Matrice 300 drone. For this reason, in all the study, will be consided only one of them, specifically the one with less favorable characteristics, as the adjustments required to make the payload compatible to one or the other are minimal.

The flight autonomy is the same as the previous drone and the dimensions and weights are slightly increased, so this changes are negligible.

The main difference is the IP rating and the resolution of the FPV camera, but these differences do not play an important role in the project and do not affect the system's performance.

The battery performance are slightly different but, as will be seen in the power budget, this will not compromise the power supply of the components.

As seen in table 2.3 where the two drones are compared, the difference in weights and payload capacities are minimal.

The IP-rating of the upgraded version of the drone provides greater resistance to water and dust.

The batteries fitted in the new version are the TB65, with an improved charging cycle of up to 400 charges compared to 200 in the previous version [23]. Some other differences are resumed in the table 2.2.

Battery	TB60	TB65
Capacity	5935 mAh	5880 mAh
Voltage	52.8 V	44.76 V
Type	LiPo 12S	Li-ion
Energy	274 Wh	263.2 Wh

Table 2.2: Differences in batteries between m300 and m350.

As far as the FVP vision system is concerned, it switches from 960p resolution to 1080p resolution with the option to activate a night vision function.

In addition, signal transmission has been increased by 5km, reaching a maximum distance of 20km for video transmission in the case of low interference and no obstacles.

2.4   Drone calculations

In order to best understand how to effectively and safely integrate our system with the chosen drone, we must start from the drone's specifications in order to make the most of its potential without affecting its operation and performance.

The starting point will be a sizing aimed at respecting the 2.7 kg weight constraint for the payload, as outlined in the high-level requirements, but some important and not negligible considerations must be made on two key aspects: the centre of gravity and the force developed during the forward pitch.

For the calculation of the centre of gravity, one must be aware of the CAD geometry constructed, the choice of components and their weight. Only then will it be possible to establish their position accurately and evaluate a possible change in weight distribution. Furthermore, the calculation of the centre of mass is facilitated by the presence of a dedicated function in the Inventor software, the code executed in matlab is only a validation of the correctness of the calculation performed by inventor.

Specification	DJIm300	DJIm350
Dimensions	Unfolded, propellers excluded, 810×670×430 mm Folded, propellers included, 430×420×430 mm	Same
Weight	3.6kg (without battery) 6,3 kg (with two TB60 batteries)	3.77kg (without battery) 6,47 kg (with two TB60 batteries)
Payload capacity	2.7kg	2.73kg
Single gimbal damper's max payload	930g	960g
MTOW	9kg	9.2kg
Max hovering accuracy	Vertical: 0.1m RTK or vision system enabled; Horizontal:0.1m RTK enabled	Same
RTK positioning accuracy	1cm+1ppm (horizontal) 1.5cm+1ppm (vertical)	Same
Max angular velocity	pitch 300°/s yaw 100°/s	Same
max pitch angle	30°	Same
Max speed	S mode: 23m/s P mode: 17m/s	S mode: 23m/s
Max wind resistance	12m/s	Same
Max flight time	55min	Same
Ingress protection rating	IP45	IP55
Operating temperature	-20°C to 50°C	Same

Table 2.3: Specifications DJI m300 and m350.

The question of the centre of gravity will be dealt with later, once all the components have been identified, but given the geometry of the system, which by necessity and use must be developed by extending forward with an injection arm, it is quite intuitable that there will be a forward shift of the centre of gravity, which must be compensated with the drone's propellers and some weight compensation by means of components allocation on the rear part.

The components introducing weight changes in the geometry are shown in table 2.4 with their respective masses and positions. Only the position in the horizontal plane is considered in the writing because it is the one relevant to the considerations illustrated. In any case, more complete information on the centre of gravity is given in the relevant CAD report files developed. For convenience and the way the system was constructed, the reference system for the centre of mass calculation is at the drone's front screw attachment.

In this table some positions are approximated due to lack of sufficient data from component manufacturers.

Component	Mass [kg]	Position [mm]
Base	0.091	-196.3
Pump	0.175	-230.0
Actuator	0.063	18.00
Arm	0.768	414.1
Tank	0.026	-275.0
Injected liquid	0.100	-250.0

Table 2.4: Mass and position of the components.

With regard to the calculation of the drone's thrust force during the pitch manoeuvre, the following reasoning was adopted: the drone is studied for a series of weight scenarios, ranging from the operational empty weight (OEW) to the maximum take-off weight (MTOW) and it is assumed that it is able to hover in each of these situations.

With this assumption, we equate the weight of the drone to the thrust force of the four propellers and make a second assumption, namely that the motors turn at a constant speed once the desired pitch angle is reached. In this position, in particular, it is the vertical component of the thrust that supports the weight. With this in mind, one simply calculates the thrust along the propeller axis and then considers the horizontal component.

All of this is implemented with aerodynamic considerations of the drag developed on the drone in the various positions assumed and the associated speeds with these inclinations. The presence of the arms of the four motors is also taken into account, constituting an area of encumbrance for the flow tube.

To be more specific, the procedure adopted was as follows:

- the geometry of the drone is established and then taken into account when calculating the aerodynamic resistance in different flight situations;

- a vector of values, representing the weight of the drone from OEW to maximum take-off weight, was created and converted into weight force in Newton;

- from this point onwards we iterate in a cycle within which we create two other vectors of the same length and biunivocally related to each other: the pitch angle vector and the velocity vector.

  Both of them start from 0 and reach the maximum value obtained from the datasheet for the respective magnitudes, so as to approximate a speed for each inclination: at zero inclination the drone will have zero speed because it is

hovering, while at maximum inclination (equal to 30 degrees) it is expected to reach the maximum speed. This however is a strong approximation because it excludes the variability of thrust given by the thrusters themselves and tends to simplify the operation of a generic drone;

- as anticipated, the next step is to calculate the propulsive thrust of the individual propeller, specific to the weight chosen at that iteration and for each angle in the pitch vector.

$$T_{singlerotor} = \frac{W}{4cos\theta} \tag{2.1}$$

Where W is the weight of the drone and θ is the pitch angle.

The thrust found must be directed, for our purposes, on the horizontal plane. It is then projected according to the sine of the pitch angle.

$$T_h = 4T_{singlerotor}sin\theta \tag{2.2}$$

- the next step involves a detailed calculation to understand the resistance created by the four arms supporting the pushing rotors and the body of the drone itself, which takes on different shapes depending on the angle of exposure to the relative current.

The resistance of the arms is considered to be the resistance of a cylinder within a flow at a certain speed, which in this case is the relative wind speed with the drone flying at a certain speed.

$$D_{arms} = \frac{1}{2}CdA\rho V^2 \tag{2.3}$$

where A is the area of the reference section of the object (in this case the 4 cylinder) orthogonal to the direction of motion, ρ is the density of the air, V the speed of the relative wind and Cd the drag coefficient, for the cylinder equal to $\frac{4}{3}$.

For the body of the drone, on the other hand, the shape can be approximated to that of a parallelepiped exposed differently depending on the drone's inclination and, as defined, the speed that develops as a result.

In general, the formula for the exposed area is as follows

$$S = hbsin(\pi/2 - \theta) + lbsin(\theta) \tag{2.4}$$

h, b and l are the 3 dimensions of the drone fuselage, respectively l the length, b the width and h the height. The drag coefficient is derived by starting from the

coefficient of a cube equal to 1.05 and arriving (again through approximation) at the drag coefficient of an inclined cube, equal to 0.8.

Putting this knowledge together, we can derive the aerodynamic resistance using the usual formula

$$D = \frac{1}{2}\rho SCdV^2 \tag{2.5}$$

- Now all that remains is to put everything together to calculate the actual horizontal thrust.

Actually, two results were plotted in graph form to assess the effect of drag and how much the results would change if drag were neglected.

So in the first results (2.3), the aerodynamic drag of the rotor arms was simply subtracted from the horizontal thrust of the four rotors, to also evaluate the effect of interference in the intake flow tube. So the equation of the horizontal thrust was modified as follows

$$T_h = 4T_{singlerotor}sin\theta - D_{arms}sin\theta \tag{2.6}$$

In the second set of results (2.4), the resistance of the drone body is also subtracted as follows

$$T_{htotal} = T_h - D \tag{2.7}$$

In both graphs, in the legend, the weight forces of the drone are marked in Newton.

It can be seen from the simplifying assumptions made that as the drone's weight increases, the curves rise because the propellers will have to counteract a greater weight and will therefore push harder.

Furthermore, the two graphs show that as the inclination increases, the horizontal component of thrust and force also increases.

Between the two graphs, which differ in their consideration of the aerodynamic resistance of the drone's body, a slight difference can be seen, which increases with increasing speed precisely because the resistance in its formula is characterised by the presence of the speed term squared.

For small angles, such as those characterising the drone's approach phase, this difference is not marked due to low flight speeds.

As will be emphasised later, with an inclination of just 5 degrees in pitch there is already more than enough force to penetrate the nest even at low payloads.

From this initial consideration the choices on the approach angle, the need to compensate for it and therefore the position, force and stroke of the actuator as well as the positioning of the arm and its fulcrum will follow.
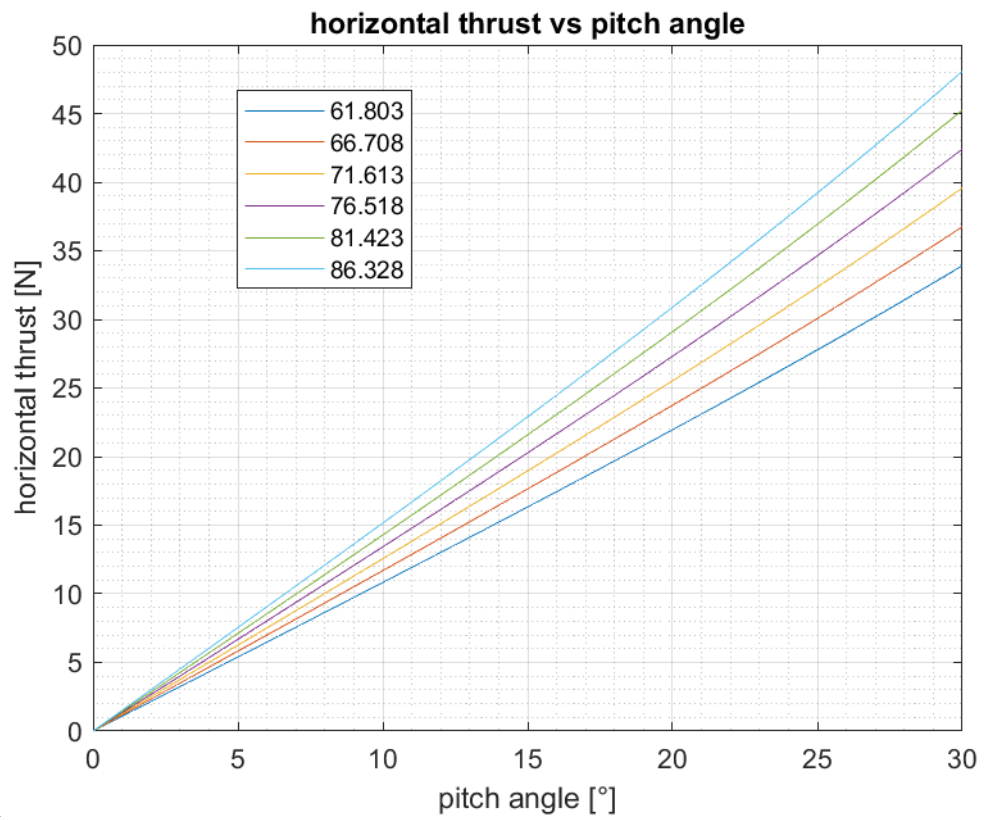
h

Figure 2.3: Horizontal thrust of the four propellers (legend: weight in N).
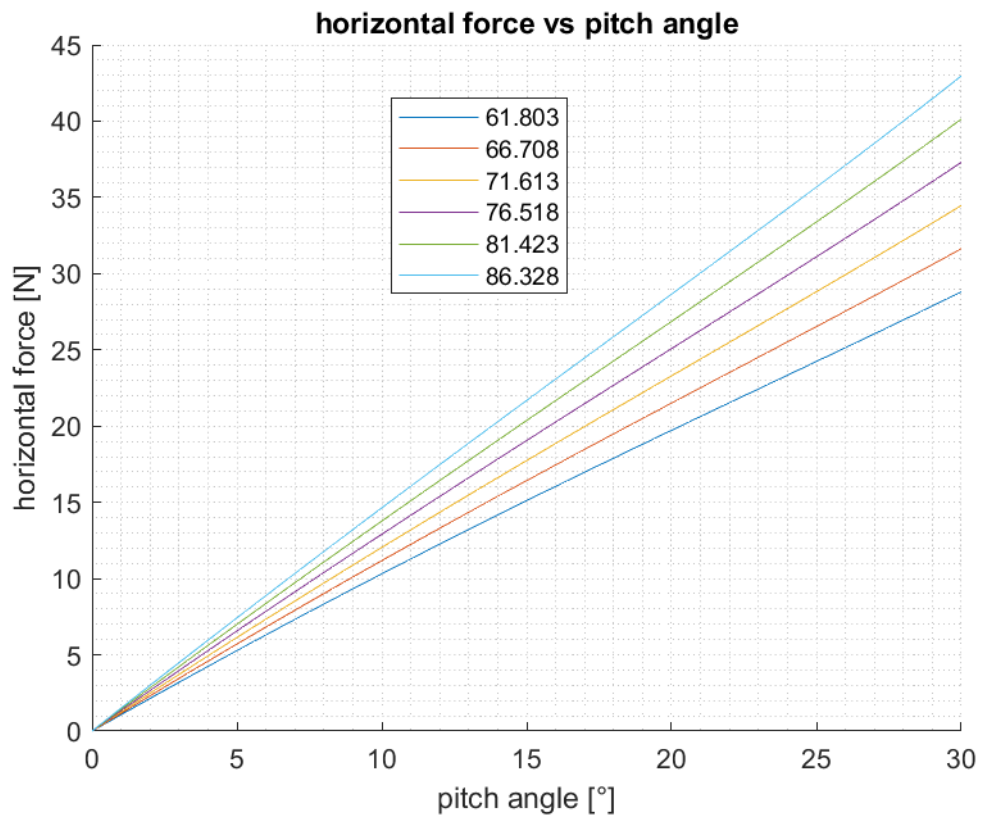
Figure 2.4: Horizontal force of the drone (legend: weight in N).

Chapter 3

Requirements

To set a list of requirements we need to analyse various aspects: the requests made by stakeholders on this project, the norms and legislation applied in this field and the constraints applied.

This phase is an iterative process that begins in the first stage with the codification of some guidelines that can set the limits for the prototype that will be created.

The first step to take is the analysis of the problem to be conscious of it and be able to choose the right approach that is not only feasible, but also more effective, so that the resources will be used in the most ecological and cost-effective way. Then obviously one must consider the stakeholders.

In this case many parts are involved and can be identified in three categories:

- The company which requests the system, in this case the professor;

- The scientific community involved in the production of the injected liquid;

- The legislation.

Title	Text	Comment	Specification	Type	Verification Method
Budget	The project shall be cost-effective and with low budget components	Stakeholder request	Mission	Mission	Review
Payload weight	The total weight of the payload shall be less than 2.7 kg	Datasheet of the drone	Drone	Physical	Analysis, Review, Test
Injections number	The drone shall be able to perform at least 10 injections per flight	Stakeholder request	Drone	Functional	Analysis
Injection	The injection shall be released inside the nest	Stakeholder request	Mission	Functional	Analysis, Review
Components	The components shell be, where possible, off the shelf components	Stakeholder request	Mission	Design	Review

Table 3.1: High level requirements

After defining these first guidelines, the base for some calculations for each component is estabilished (detailed in others chapters).

Each component will be added in the product tree of the project and will define a new set of specific constraints and requirements necessary to be functional and operate in the design conditions.

The legislative requirements have not been dealt with in this thesis as the basic legislation on drones has already been abundantly reported on the use of drones and their classification according to weight, risk and operation, so reference will simply be made to the regulations in force in the category in which the drone falls and expressed by ENAC for Italian territory and EASA for European territory.

3.1 Requirements definition

The remaining requirements (which are given in the annexes) are gradually added into the list of high-level requirements (derived directly from stakeholder impositions and consequences closely linked to these impositions, of which the table 3.1 is an example).

The difference between the first and the lowest level requirements is that the latter are also obtained as a consequence of the choice of components themselves and as a result of preliminary calculations for structural dimensioning and selection of physical components directly from the market.

As we have also seen from the example table given for the first, higher level requirements (3.1), the requirements are expressed using a formal manner, by means of a standard that provides for each one a unique and identifying code (generally an alphanumeric code), a title of the requirement that immediately and clearly identifies its content, a sentence in the "shell" form expressing the requirement, a comment identifying its origin and the reason for imposing it, a specific category, the type of requirement that categorises it and a verification method according to which the requirement can then actually be verified in the final phase by means of 4 main methods: analysis, review, test or inspection.

The four types of verification outlined above are distinguished according to their applicability:

- the analysis method, probably the most widely used at this stage, enables precisely the data imposed as requirements to be analysed by means of calculations and verification software;

- the inspection method consists of an actual physical inspection of a part, a component, and its nameplate data;

- the review method is a simple check on compliance with the requirement by supervising what has been done;

- finally, the test method allows real, practical tests to be carried out on the physical components, and this is only possible at an almost final stage of the project, where it is possible to actually lay hands on the physical parts.

With regard to the definition of the requirement at this preliminary stage, it is common for not all requirements to be expressed in a definitive manner but only in an indicative and approximate manner, especially with regard to the electrical and control part, which is not the focus of this work.

The purpose of a project is then to arrive at a definitive writing of the requirements in later stages, implementing or even correcting some of those initially written following calculations and verifications.

Chapter 4

Pump

The pump is the most important component of all the hydraulic system because it has the duty to push the liquid from the tank along the entire arm up to the nest.

To choose the pump firstly a study was conducted on the different types of pumps to know which one, with its specific features, would be more appropriate to the requested task.

The injections to perform require a small volume of fluid per nest, about 10ml, resulting in a very low required flow rate. Then, the second aspect to consider is the pressure required to make possible the injection through a 2m long tube with a very small diameter: some calculation on the losses has to be performed.

Finally it is known that each injection is separated from the others, so the pump has to operate in an intermittent way.

After this consideration, and after extensive market research, two possible pump configurations were selected. These two solutions are suitable for this kind of applications: the peristaltic pump or the diaphragm pump.

4.1   Peristaltic pump

The peristaltic pump, also known as hose pump, tube pump or roller pump, finds use for a big variety of applications involving liquids of different viscosities and densities across multiple fields, like alimentary production, pharmaceutical applications and also all the activities which involve the distribution of a substance in a partialized way, even in small volume [24].

It is a volumetric pump which functioning is based on the use of the peristalsis principle: the device creates an occlusion that is able to generate a negative pressure and at the same time phyfically pushing the liquid in the forward section away.

To perform this function, the pump requires a flexible tube compressed by some rotating rollers (at least 2) so that the effect is similar to a squeezed tube. These

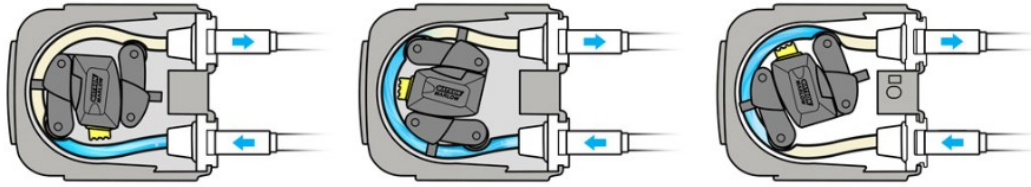rollers are mounted on a rotor moved by an elecrtical motor.

Figure 4.1: Peristaltic pump working principle [25].

As depicted in the figure 4.1, the roller compresses the tube creating a negative pressure actracting the fluid into the hose, this occurs because, after compression, the hose section regains its original form. In the main time, the next roller pushes the liquid toward the pump outlet and repeats the process for the next portion of liquid, preventing any backflow.

The number of rollers is important for two conflicting parammeters: the flow rate and the pulsation. Less rollers result in a higher flow rate, while increasing the number of rollers the flow rate will decrease but the pulsation of the fluid will be also reduced, giving a more constant fluid output [25].

The hose of this type of pump is the most critical component, because it has to be resistent to chemical and mechanical actions. The first type of resistence is given by the fact that the hose is the only part in contact with the fluid and has to be chemical compatible, even if the corrosion potential of the fluid is high.

The seal-less construction prevents fluid leaks. In this way the maintenance time of the pump is reduced, because pump elements are not exposed to abrasion deriving from possible contact with the transported fluid [24].

The mechanical stress given by the physical action of the rollers has to be managed by the hose through its elasticity. For this reason the hose is, most of the time, made of PVC materials or silicone.

Nowadays this pumps are realised in such a way to be easy to mantain, so the hose is easily removable via a counter for replacement in case of reduced elasticity, corrosion or damage. In addition, this pump contains fewer mechanical components rather than other pumps, reducing the worn parts.

To control a peristaltic pump we can [26]:

- select a reducer

- use a line start on/off controls

- use a PLC

- use a VFD to control the speeds

In conclusion, this pump is particularly useful in all those applications where the liquid (for contamination or hazardous reasons) should avoid direct contact with the pump. It can also handle high viscosities and fluids with solid dispersion, precisely because the pushing force occurs by deformation of the pipe.

The interesting thing for the project is that the pump allows the flow rate regulation through repetitions per minute (RPMs), enabling liquid dosing.

It is also worth mentioning the fact that it is self-priming and that even at no-load, as is the case at the beginning of the operation, it is not damaged during dry running.

Several disavantages of this technology are mentioned below [27]:

- the system must be calibrated to have a specific accuracy because the tube is variable;

- the tube have to be changed after some time to prevent leaks;

- the pulsation is unavoidable, can only be reduced;

- the flow rate is sensitive to pressure conditions;

- the dispersion of solid particles can reduce the effectiveness of the pump.

4.2 Diaphragm pump

The diaphragm pump, also called membrane pump, has a different way to operate. It relies on a membrane (or a duble membrane) operated by using a shaft or compressed air directed back and forth inside the pump's core [28]. This thecnology is able to convert the mechanical or hydraulic energy into dynamic pressure.

These pumps are also capable of handling liquid with different viscosity levels and with dispersions of solid particles.

Basically it is divided in two main parts: transmission and pumping unit.

The pumping unit is the one that encloses the rest of the pump, i.e. the diaphragm, pumping chamber and the two valves (suction and delivery valve).

The transmission transfers mechanical energy from the motor,in this case an electric motor, to the pump which converts this energy into fluid pressure [29].

As mentioned above, the movement can be imprinted in various ways: pneumatically via compressed air or mechanically using lever or cam systems.

They are generally employed in small or medium ranges, which makes them ideal for our type of use, and this idea is also supported by the analysis of other papers on the use of drones in agriculture.

Membranes (or diaphragms) can be made of various materials, in any case plastic and elastic. Their function is to create negative pressure to draw the liquid into the chamber and push it into the delivery manifold, but at the same time they allow the separation between hydraulic part and the pneumatic/mechanical ones, preventing interactions that could alter the fluid or damage the pump.

The Fluid Chambers, on the other hand, house the volume of liquid drawn and pushed through the diaphragms in each cycle, along with non-return valves required to avoid backflow. These valves, in miniature pumps, are brought into place by springs so that they do not depend on the orientation of the pump, whereas in larger pumps everything relies on gravity.

If the pump is pneumatically driven, the central part must also include valves for the air to direct and move the diaphragm itself, with an outlet and an inlet for the compressed air, and in the case of the double diaphragm, an additional valve that directs the air to one chamber or the other.
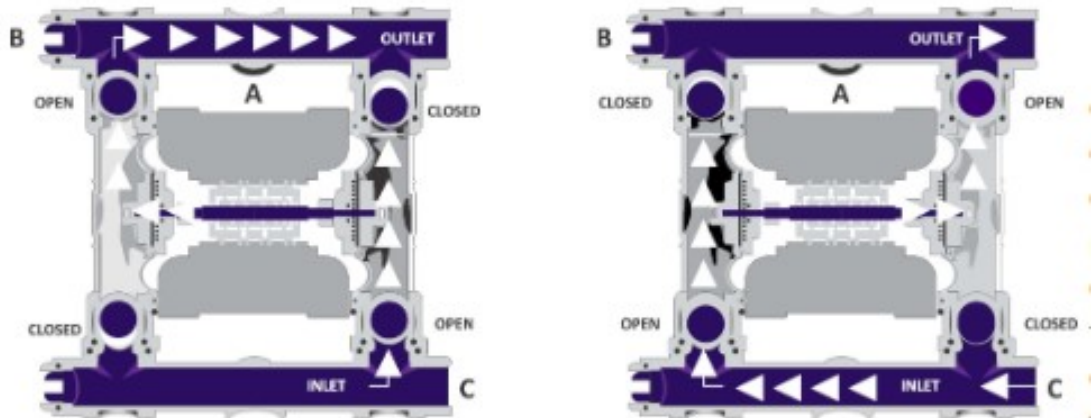
Figure 4.2: Air operated double diaphragm pump operation [30].

Apart from the fact that the diaphragm pump shown in the figure 4.2 is pneumatically driven (whereas the one in use for the project will be electrically driven), is interesting to see its operation schematically in order to understand it better.

In a diaphragm pump, two manifolds for suction (bottom of the picture 4.2) and discharge (top) are visible.

There are two phases called "strokes" (4.4): the first is a suction phase, in which the diaphragm (in one of the two chambers) retracts, creating a negative pressure that opens the lower valve and keeps the upper one closed, thus causing a volume of liquid to enter the chamber through suction. In the next stroke, the diaphragm moves forward compressing the volume of the chamber it faces: in this way the

valves will reverse their behaviour, so the upper one will move allowing the fluid to pass through and the lower one will close. The second membrane, connected to the first in the case of a double membrane pump, will have complementary behaviour and will therefore allow its chamber to empty and refill in counter-phase to the first, optimising pump operation.

The mechanical transmission shown in figure 4.3, will be explained in order to understand what enables the movement of the membranes with the sole purpose of being complete in the description, since in the project the pump is not made by us but bought, so we will not deal in detail with the parts but with the operational logic.
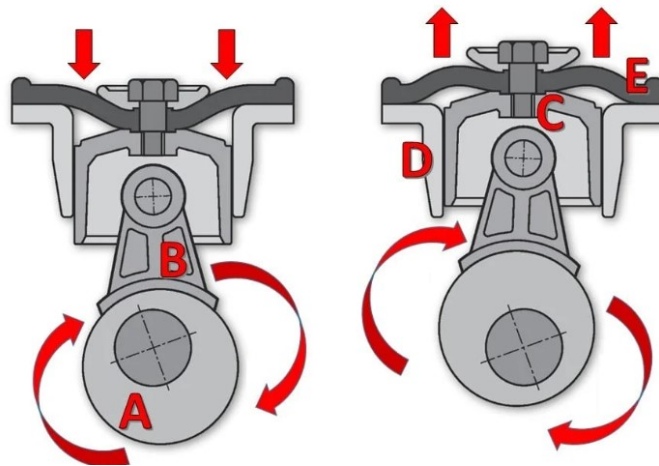
Figure 4.3: Diaphragm pump transmission [29]

The electric motor supplies energy via a shaft that is converted from rotational to oscillatory motion using a crank-rod system connected to the shaft with a certain eccentricity and moving a piston (inside a case) linked to the diaphragm.

The utilization of diaphragm pumps has considerable advantages, which are mentioned below.

- The division between the two sections of the pump, as already mentioned, gives the advantage of avoiding contamination of the pumped liquid and wear and tear on the mechanical parts of the pump, extending its life and reducing the number of maintenance operations required.

- From this first advantage also follows the possibility of pumping liquids that are chemically aggressive, dirty or contain solid particles within them. Furthermore, the pump itself is capable of handling high-density liquids.

- It is applicable in a wide range of operations and sectors, operating at high efficiency, and for different flow rates due to its adaptability.

- This type of pump also has the ability to withstand dry running, situation that can occur during start-up when the supply line is initially only full of air, or in the event of a rupture where there are leaks and thus air pockets.

- Head capability: it can draw in fluids from lower levels than the pump because it creates a vacuum on the suction line by creating a hermetic seal with the diaphragm.

- Self-priming capability: the pump can start with an empty suction pipe without damage and automatically expels the air inside during start-up.

- The pump pauses when there is no flow and there is no energy consumption: all is managed by the valves.
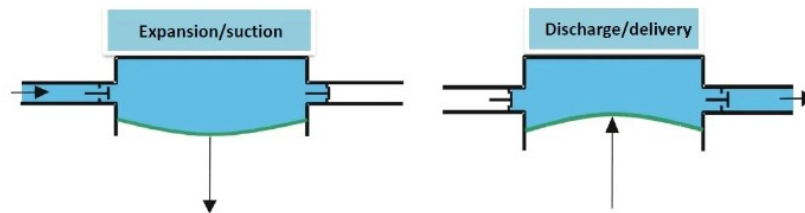
Figure 4.4: Membrane or diaphragm of the pump

Unlike the peristaltic pump, where two components are separate (tube and rollers), the division between the two zones in this pump is not marked by physical boundaries and one must be careful of possible leaks in two particular areas: the boundary between the central zone and the diaphragm and the boundary between the central zone and the mainfolds. [31]

The installation of this type of pump can be done in various ways. Due to its self-priming and dry-running capability, the pump can be positioned above the level of fluid it has to draw: the maximum height is determined by the head and leakage.

This is the mounting scenario of interest, but there are not particular problems as the heights between suction and fluid are in the order of few centimetres.

The pump could also be installed below the fluid level or submerged, but the latter configuration is more suitable for different applications as it would result in a reduction of aviable tank volume without any particular advantage and, indeed, greater construction complications.

The other installation configurations were not used but are mentioned for completeness and future possibilities, especially the possibility of drawing liquid from two different tanks.

The pump can work with two fluids simultaneously (provided they have similar viscosity and physical characteristics) by splitting both delivery and suction. With the separate suction option, the pump can also be used as a mixer. [28]

The pump can be controlled by switching on and off the electric or air motor that controls the transmission.

4.3 Pump calculations

The definition of the pump's characteristic quantities, in order to have the parameters to select from catalogues a solution, was done using calculation codes.

These codes take into account approximate quantities, considerations from previous projects and theoretical and empirical formulae many times obtained from sources such as manufacturers of these components, which allow experimental calculations to be made in order to determine the most suitable solution.

In a first iteration of calculations, defined and chosen values were brought in, including those derived from investors or the scientific community. In a second iteration, variability and uncertainties (such as the volume of liquid in each injection and the number of injections) were then contemplated in order to test how much these uncertainties impact on the result and the ultimate choice of components.

The full calculations with the Matlab code are given in the appendix, but the fundamental steps of the procedure are given and commented below.

As defined, each injection is about V=10 ml of liquid (with an uncertainty of 2ml). Estimating a very short running time of the pump during injection (4 seconds, based on observation of Fitobiotecht's operations seen in the videos), the necessary liquid flow rate is determined through the simple calculation of the volumetric flow rate:

$$flow = Q = \frac{V}{t}[m^3/s] \tag{4.1}$$

Converting the quantities into hydraulic units, the liquid flow ranges between 0.12 and 0.18 liters per minute (including the uncertainty on the volume injected).

It is pointed out that these calculation uncertainties also impact other aspects of the design, because the volume of liquid to be transported varies from 80ml to 120ml, and for this reason it will be convenient to provide a larger reservoir or an operational stage of pipeline pre-filling.

The characteristics of the liquid are crucial for the calculations. The liquid is assumed to be very similar to water (with the distinction that it contains solid particles in suspension but which are not said to create agglomerates).

Water density and dynamic viscosity values are used

$$\rho = 997 \frac{kg}{m^3}$$

$$\eta = 1.002e - 3\frac{kg}{ms}$$

Potential losses must be calculated, so pipelines are examinated.

There are not many assumptions to be made, at least after a few iterations: once the pump is chosen, the cross section of the pipe is pretty much chosen because manufacturers associate and recommend particular piping for pumps on the market.

The pipe material is defined and its internal roughness too.

The length of the conduit and the presence of bends are determined once the geometry is defined in the CAD with the relative positions of the various elements.

To be conservative we will assume a pipeline of

$$l = 2m$$

(1.2 meters only for the arm and the others assumed as belonging to the section between tank and pump and between pump and injection arm).

The inner tube diameter is

d=3.5mm

In addition, the use of a sanitary-type needle at the tip of the arm is assumed.

This clearly represents a narrowing of the section, resulting in possible clogging by agglomeration of suspension of solid particles, but that is ruled out for now and is not particularly important because of the ease of replacing the final needle even with solutions larger in internal diameter (for which, however, the necessary force for nest penetration must then be studied).

The effect that shrinkage has on pressure is calculated along with the various losses.

As for the needle, you want to use solutions that are readily available, inexpensive and easily replaceable. For size and characteristics, canula needles are suitable choices in the market. The system used to encode the inner diameter of the needles is the "gauge" in the medical field, a non-international system.

According to ISO convention, the needles are classified by color, diameter, length and flux as the taable 4.5 illustrates.

Figure 4.5: Cannula types classification [32]

The cannula needles can go to 34 gauge up to 7 gauge. The 34 gauge is the smallest one in diameter while the 10 gauge is the largest one. The 16 gauge one was selected.

Regarding needle length, there are different measures: 25, 32, 38 and 50mm.

According to the available flow rates per needle of various sizes in internal diameter, and estimating that the required flow rates of our project range from a minimum of 0.12 l/min to a maximum of 0.18 l/min, the 16 gauge needle is suitable.

size	inner diameter [mm]
17	1.067
16	1.194
15	1.372
14	1.6

Table 4.1: dimensions of the needles [33]

Then, considering the cross-sectional areas (the needle one is displayed in table 4.1), one can easily calculate the flow velocity inside the duct applying the flow

conservation principle: obviously for small cross-sections the flow velocity will have to increase to maintain the flow rate.

$$v = \frac{Q}{S}[m/s] \tag{4.2}$$

The highest velocity is in the smaller section, i.e. in the needle, where the maximum flow rate corresponds to around 3.82 m/s (reliable datum compared via online research with characteristic syringe fluid exit velocities).

Then, using Bernoulli's equation,

$$p_1 + \frac{1}{2}\rho v_1^2 + \rho g h_1 = p_2 + \frac{1}{2}\rho v_2^2 + \rho g h_2 \tag{4.3}$$

the internal pressure is calculated using the available data and assuming the height difference to be negligible because it is only a few centimetres.

$$p_1 + \frac{1}{2}\rho v_1^2 = p_2 + \frac{1}{2}\rho v_2^2 \tag{4.4}$$

where 1 corresponds to the cross-section of the tube and 2 corresponds to that of the needle.

Having previously calculated the velocities in the different sections, knowing the density of the fluid and imposing the pressure at the outlet of the needle equal to the external ambient pressure (for now left at the value of ambient pressure at sea level) we are able to calculate the internal pressure of the pipe, which lies in a range from 1.045 bar to 1.086 bar.

To this preliminary calculation considerations of internal losses due to dissipation and friction will be added.

To this end, we calculate the Reynolds in both the pipe and the needle to understand the nature of the flow, whether laminar or turbulent, and then apply formulas for calculating losses.

$$Re = \frac{\rho v d}{\eta} \tag{4.5}$$

The maximum Reynolds values in the tube and needle are respectively 1086 and 3801.

This information is used to calculate the distributed losses in the pipeline.

In the pipe, the Reynolds number is less than the critical value of 2300, so there is laminar flow.

Then the pressure loss is calculate as follows, already reporting the estimated pipe length so that we have the final result.

$$\Delta p = \lambda \frac{L \rho v^2}{2d} \tag{4.6}$$

Where λ is the friction factor, which for laminar regime is

$$\lambda = \frac{64}{Re} \tag{4.7}$$

The losses in this case do not exceed 2000 Pa and are therefore relatively negligible.

These equations are experimental and compared across multiple sites as well as from prior knowledge in aerodynamics, gasdynamics, and fluid dynamics courses [34] [35].

The turbulent case is more complex because the equations previously used for the friction factor no longer applies.

The friction factor, in this case, is not constant and depends on three main factors:

- Reynolds number,

- relative roughness (i.e., the presence of internal asperities in the duct) which has the following mathematical expression $\frac{\epsilon}{d}$, where ϵ is the roughness i.e., the average height of the internal imperfections and d is the internal diameter.

To find this value Moody diagram (4.6) or appropriate tables with tabulated values for Raynolds and roughness are used.
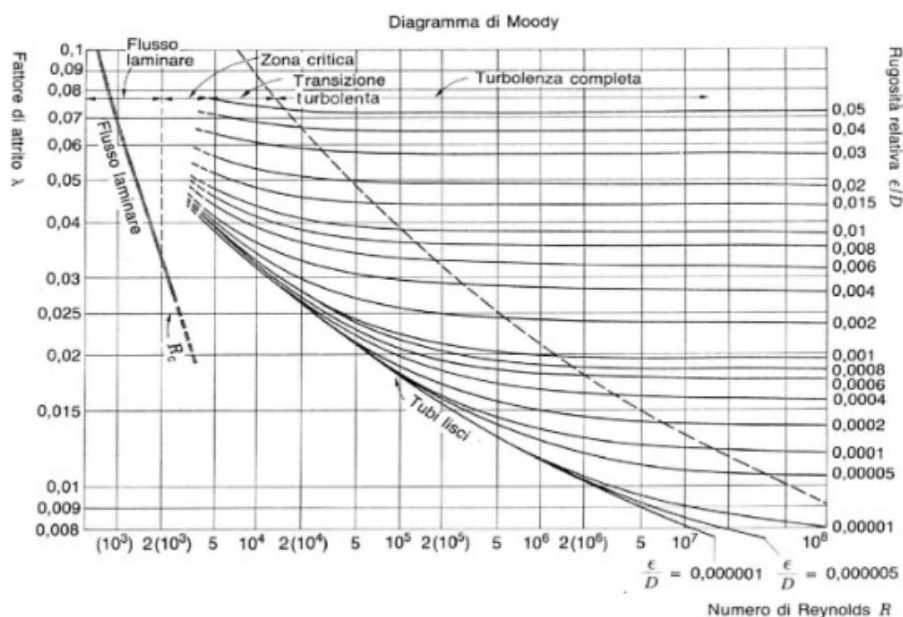
Figure 4.6: Moody diagram [35]

Actually the value obtained in the needle case does not correspond to a fully turbulent case but to a transition case between the two fluid regimes. Therefore a

turbulent case is assumed to have a worst case scenario, with a Re value of 4000 that initiates the turbulent case.

Assuming an $\epsilon = 0.046mm$ for commercial steel and using the digram we obtain a friction factor $\zeta = \lambda = 0.08$, (not so easy to read from the diagram).

From another experimental calculation [36]

$$\lambda = 0.07Re^{-0.13}d^{-0.14} \tag{4.8}$$

From here, by entering ζ instead of λ and needle data instead of tube data in the loss formula we again obtain negligible loss values (the maximum is about 3e4 Pa).

In the end the concentrated losses are introduced, in the section reduced in the connection between tube and needle.

$$\Delta p_{local} = \beta \frac{v^2}{2} \rho \tag{4.9}$$

with β friction factor, which in the case of sudden shrinkage given by sharp-edged inlet is worth 0.5.

Even in this case the local losses are not relevant, with a maximum of about 24 Pa.
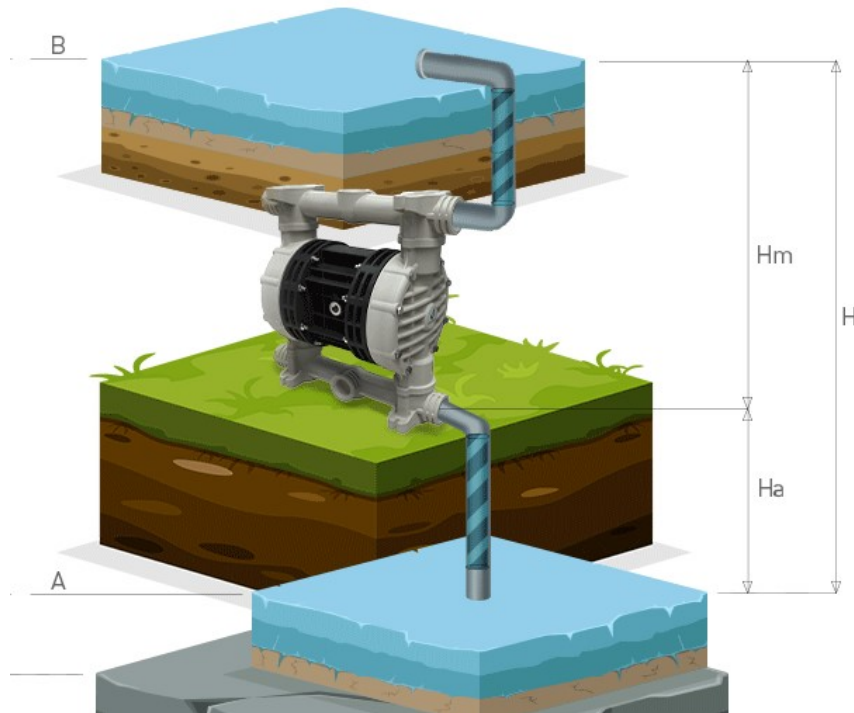
Figure 4.7: Head [36]

For the head, relative positions must be defined between the pump, reservoir and delivery and suction of the pump itself.

As in the figure 4.7, Ha is the geodetic suction height, i.e. the height between the suction inlet and the pump inlet, Hm the geodetic delivery height, i.e. between the delivery and the pump outlet, and H the geodetic head, i.e. the difference in height between delivery and suction, which is nothing more than the sum of the previous two.

Now it needs to be verified whether the sum of barometric pressure and geodetic pressure drop is greater than the characteristic NPSHr of the pump obtainable from the datasheet (in our case NPSHr=3m) added to the previously calculated pressure drops (Y) and the vapour pressure of the liquid.

Obviously, pressure values must be converted into metres, considering that 1bar is approximately 10m.

For the vapour pressure of water, on the other hand, one either has the tabulated value or uses the empirical formula

$$p_v = \frac{6.11}{1000} * 10^{\frac{7.5T}{237.7+T}} = 0.0233 bar \tag{4.10}$$

In conclusion it is proved that

$$p + H > NPSHr + Y + p_v \tag{4.11}$$

4.4 Pump comparison

Here is shown the table 4.2 containing the various pumps, which was useful in a selection process for this component in order to visually have a direct comparison of the various parameters.

Graphical representations (figures 4.8 and 4.9) were then created on this basis showing the values of the key parameters for selection.

name	pressure [bar]	flow [l/min]	weight [g]
kk300-st	2	0.485	483
15ks	2	1.072	405
15qq	2	1	405
fp70	2	0.85	285
ltc	2	1.5	333
16k	2	0.14	85
16k	2	0.16	60
19k	2	0.7	175
10kd	2	1	185
3k	2	1.5	385

Table 4.2: Pump comparison table
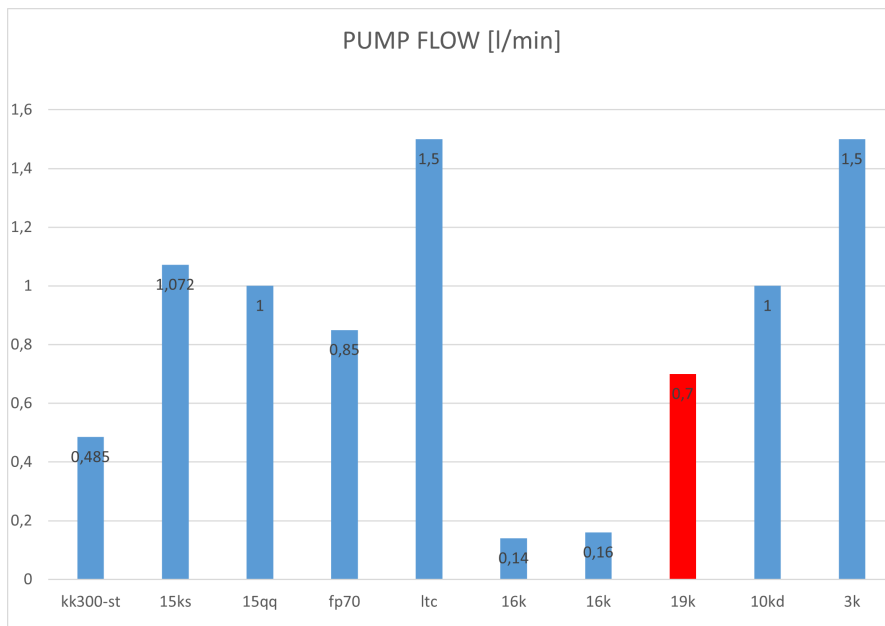
Figure 4.8: Pump flow comparison
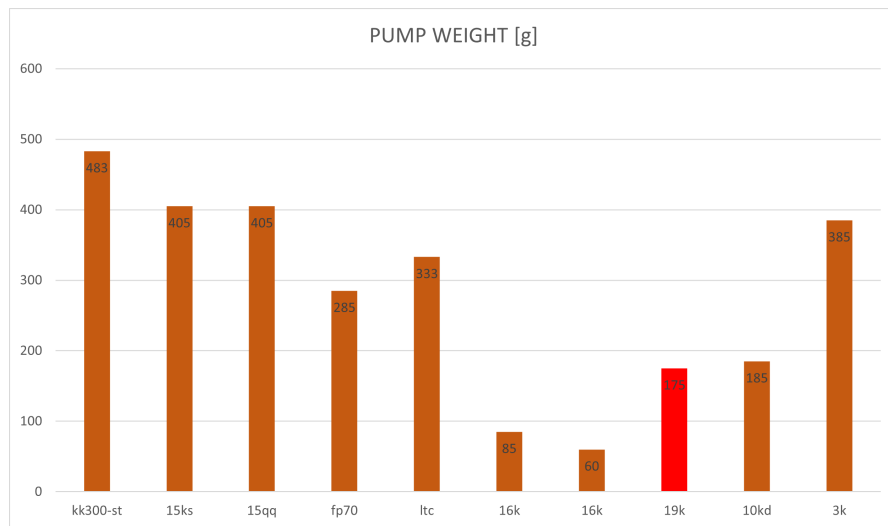
Figure 4.9: Pump weight comparison

Chapter 5

Actuator

This thesis work is not the first in the field of invasive insects. As said before, two other known companies developed similar systems.

The innovation in this product lies in the fact that the arm can be moved.

The main purpose of this innovation is to compensate for the pitch angle during two different phases: the approach to the nest which induces a pitch down for the drone, and the departure once the injection is completed, causing a pitch up for the drone.

Previous works were based on a flexible structure. In the case of an agricultural operation drone, this can be acceptable because the structure of the drone has a large distance between the different propellers. In the case of the DJI m300 and m350 the use this type of structure is not feasible, due to the fact that the drone was designed for industrial operations and not for a complex and large payload as the one we want to realise.

The propellers are closer one to another, and they are not common traction propellers, they are pushing propellers so they are under the main plane of the fuselage of the drone, near the system.

For these reasons we can not have a flexible solution that could cause the impact between the arm of the injection system and the propellers.

The main idea to compensate for this angle creating the needed movement is to move the arm with a linear actuator. This solution is preferred over a classic electric motor because it is light, compact and it can be implemented easily in the CAD solution providing a momentum arm that can reduce the force needed by the actuator itself.

5.1 Actuator calculations

Is important to consider how the whole system will work once it is assembled and operative.

As was said before, the drone needs to pitch down during the approach. Meanwhile the arm shall be maintained in the horizontal plane to maximize penetration force and achieve the optimal situation: a mechanical system of movement to compensate the pitch of the drone is required. In the same way, compensation is needed for the pitch up of the drone during the departure manoeuvre.

The crucial thing to evaluate before all this is the horizontal force needed to penetrate the nest.

The nest is a soft multilayered silky structure, so it should be easy to penetrate.

As a common medical needle is considered, which is useful to reduce the force needed because the penetration area is minimised, there is the advantage of having a part that is very cheap, easy to find and to replace.

Some studies about this kind of needle suggest that the penetration force needed in muscular tissues is about 1.6N using old 23 gauge needles [37]. To be conservative the use a bigger needle is supposed, but the nest should be even less resistent to penetration requiring even less force.

To be sure about the penetration, and to account uncertainties in the drone movements characterized by sudden movements in pitch that can not be defined with an high accuracy (due also to the presence of the payload to compensate and turbulences and wind), an inclination of the drone of 5 degrees is considered.

As a result, a 5N force (see 2.4) is developed, that is way above the force needed to penetrate the nest.

For the calculation procedure refer to chapter 2.

5.2 Leverage type

Two different configurations based on the type of leverage are possible:

- first type leverage: based on the fact that the pushing force (so the actuator) is located behind the pivoting point;

- second type leverage: based on the fact that the pushing force (actuator) is located after the pivoting point.

Some studies on the moment generated, based on the force of the actuator, were realised changing pivot point or application force point.

Since the arm has a length of l_{arm} =1.2m and therefore the centre of gravity is about halfway (i.e. 0.6m), we will vary the point of application from 0 (connection

between arm and drone) to the middle of the arm, where the centre of gravity is located.

In the code will be created a vector of the distances, which calculates for each point in this range the generated momentum, the linear and angular displacement, and the respective velocities.

Data for the chosen actuator were reported (always after an initial dimensioning phase of realistic values to help us, as was the case with the pump, to choose and orient ourselves during the first steps).

The chosen actuator has a maximum stroke (s) of 60mm, in the code it is setted at mid-stroke so that the arm orientation can be adapted in both approaching and receding, reserving an equal stroke for the reverse manoeuvre.

The travel speed of the actuator arm is 5.8 mm/s, which means that in 5 seconds it is able to reach the end of its stroke starting from mid-position.

The last fundamental value is the force it is able to develop, which is 50N dynamic (and goes up to 75N in static conditions, i.e. holding position) [38].

Imposing a lower limit on the force, which is equal to the weight force of the arm, the two lever configurations are separately analysed and then compared.

For both configurations, the moment based on the force application point (for the third type leverage) or the pivot point (for the first type leverage) is calculated.

$$M = F_{motor}l \tag{5.1}$$

in the equation l is the variable distance between application point and pivoting point.

The moment developed by the actuator must obviously be greater than the opposite torque generated by the weight of the arm itself, which counteracts the upward movement of the arm.

In the case of the first type of lever (pivot point being mobile and point of application of the force fixed at the end of the arm) there is a visible advantage in the trend in figure 5.1. As the pivot point approaches the centre of gravity, the arm of the weight force is reduced and consequently the torque created by it, requiring less effort from the actuator.

$$M_{arm} = (\frac{l_{arm}}{2} - l)m_{arm}g \tag{5.2}$$

For the third type of lever, however, it is only the actuator that moves, so the arm of the weight force remains visibly unchanged in the graph 5.2.

$$M_{arm} = \frac{l_{arm}}{2}m_{arm}g \tag{5.3}$$
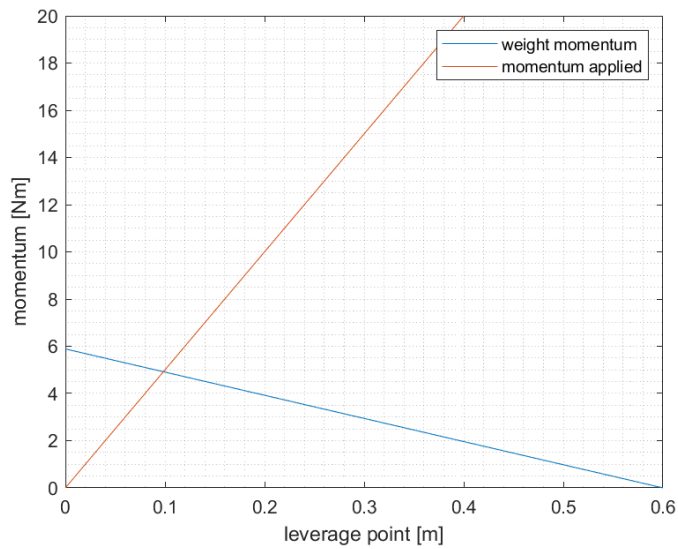
Figure 5.1: Momentum in first type leverage.
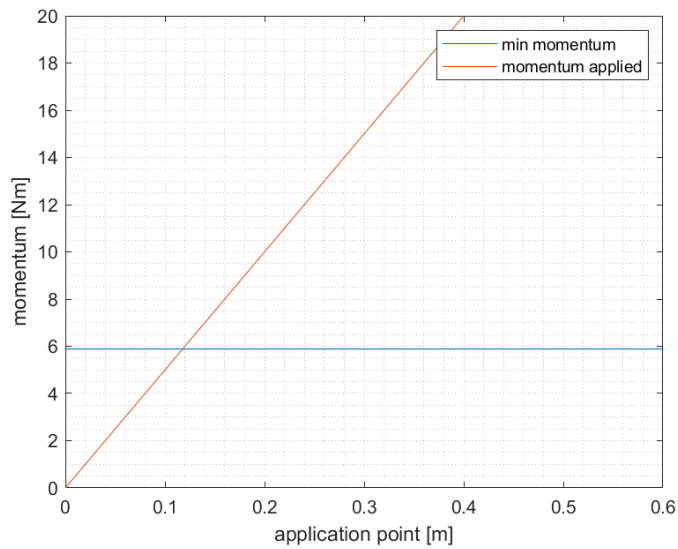
Figure 5.2: Momentum in third type leverage.

As is shown in the graphs 5.1 and 5.2 the first leverage type configuration is more convenient for the force required for the reason explained before, allowing a reduced arm for the force that must generate the torque.

The next phase was the comparison of the linear actuator displacement and the linear actuator speed. In this part the calculations are only geometric and trigonometric considerations.

Angular and linear displacement and their respective velocities are calculated with the following formulas.

$$d_{needle} = sin(atan(\frac{s}{l}))x \tag{5.4}$$

$$ad_{needle} = atan(\frac{d_{needle}}{x}) \tag{5.5}$$

$$ds_{needle} = \frac{d_{needle}}{t} \tag{5.6}$$

$$as_{needle} = \frac{ad_{needle}}{t} \tag{5.7}$$

Where:

- d=linear displacement

- ad=angular displacement

- ds=linear speed

- as=angular speed

- t= attuation time of the actuator to run the stroke imposed

- s=displacement of the actuator (stroke)

- l=application point of the force (leverage 3) or position of the pivot (leverage 1)

- l_{arm}=arm length

- x=$l_{arm} - l$ (leverage 1) or x=l_{arm} (leverage 3)

The first equation for linear displacement could be directly calculated using the tangent, but in doing so an approximation is introduced, using the sine and the arcotangent, in order to eliminate the infinite values that would result from the fractions with null values at the denominator in the ratios between the cathexes of the virtual triangles created by actuator displacement and injection arm.

In this regard, however, the first sections up to a value of approximately 0.1m abscissa are not considered reliable in the graphs.

The rest of the values are reliable and do not deviate from the actual result.

From the andaments in the graphs 5.3 and 5.4 of the linear displacement and linear speed is clear that there are not so many differences in the two configurations compared.
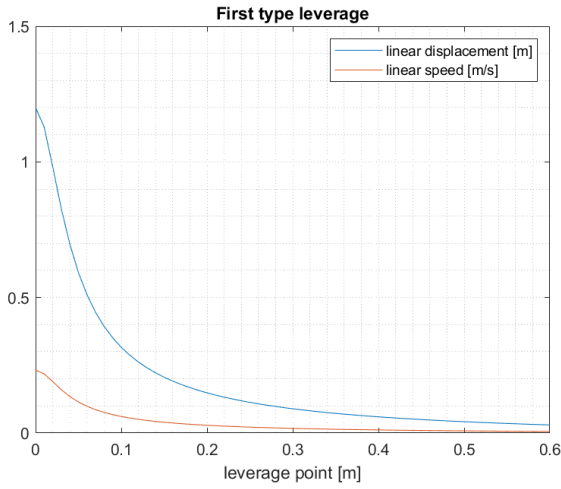
Figure 5.3: First type leverage linear quantities
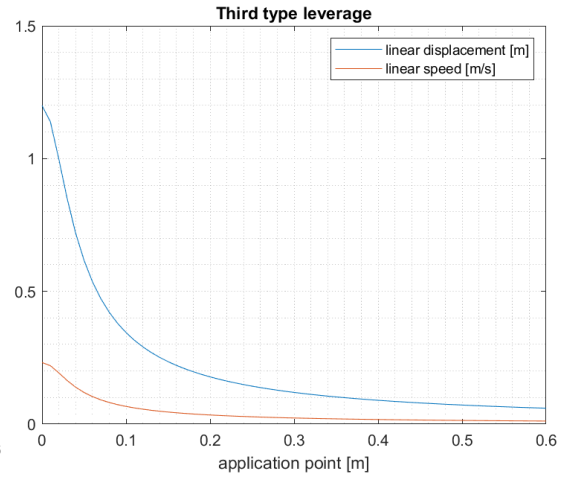
Figure 5.4: Third type leverage linear quantities

More important are the graphs of the angular displacements and angular speed (5.5), to be compared with the horizontal force graph to understand if the system, with the displacement given by the actuator in the position and configuration chosen, is able to compensate for the needed pitch.

For the application point chosen a 5 degree displacement angle can be handled without any issues as it will be now shown.

The actuator is positioned at a distance of 20 cm from the pivoting point.

By doing so, an higher margin is considered for the developed torque than that required in both lever configurations analised.

As a matter of fact, in the graph of the horizontally exchanged force between drone and nest, a lower limit of 5° for the drone's pitch is setted (sufficient from the analyses made to develop the required penetration force).

However the graphs of the angular displacements of the levers reveal that the configuration can develop an even greater compensation. Specifically, at 0.2 m lever arm, an 8.44° angular displacement is developed for both configurations.

In point of fact, it can be seen from mathematical reworkings that the angular displacement is the same, it only changes how compact the system can be and therefore how much the arm between the lever and actuator can be reduced considering the reflections made on the momentum.

On this basis, a third type of lever is chosen.
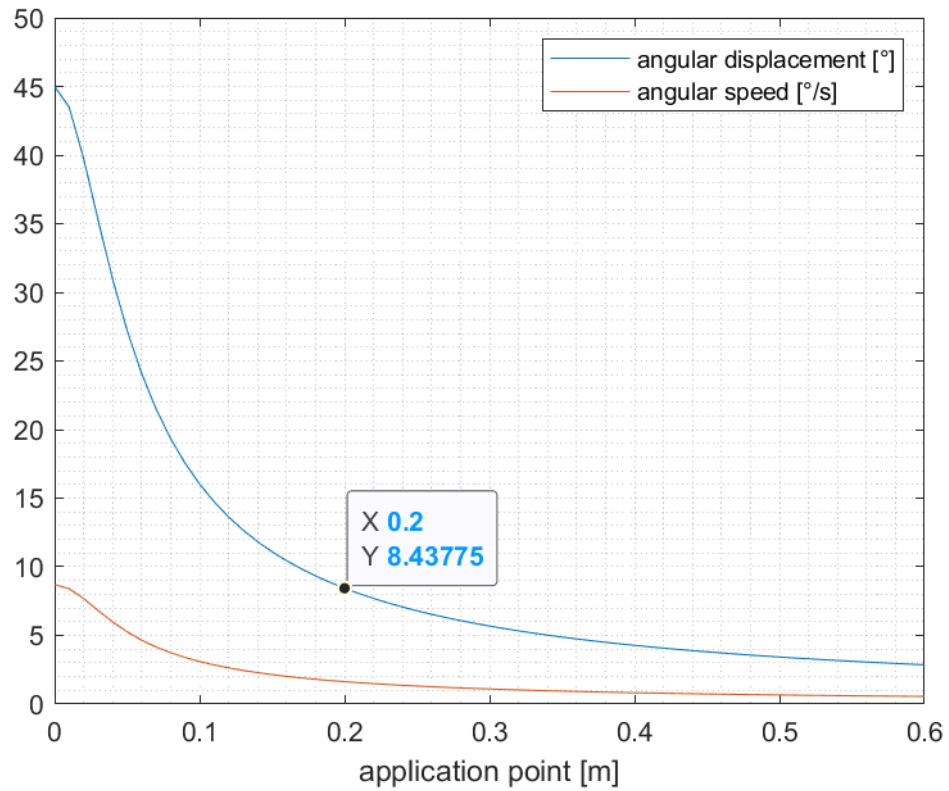
Figure 5.5: Angular desplacement and speed.

5.3   Actuator comparison

Here are shown the graphs 5.6 and 5.7, containing the various actuators, helpful in a selection process for this component in order to visually have a direct comparison of the parameters.
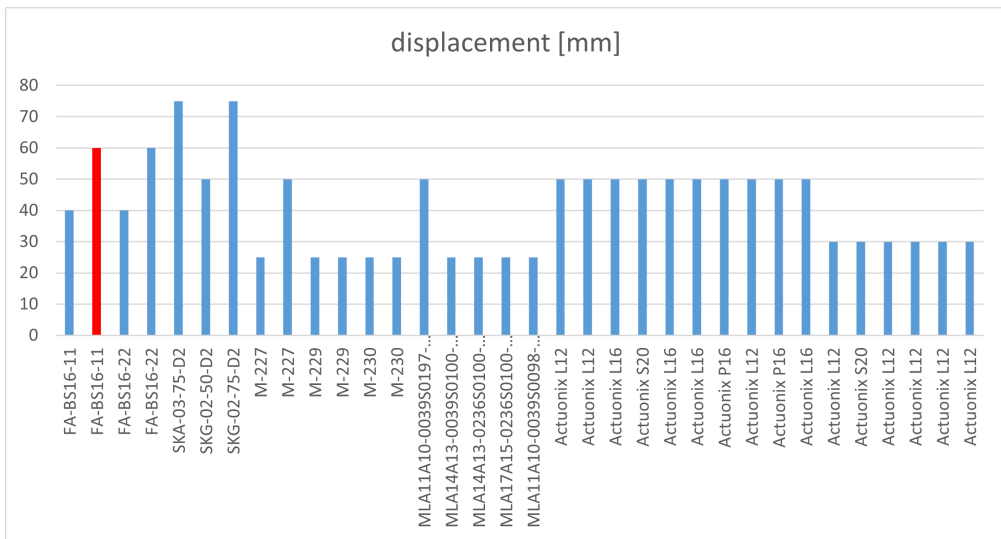
Figure 5.6: Actuators displacement comparison.
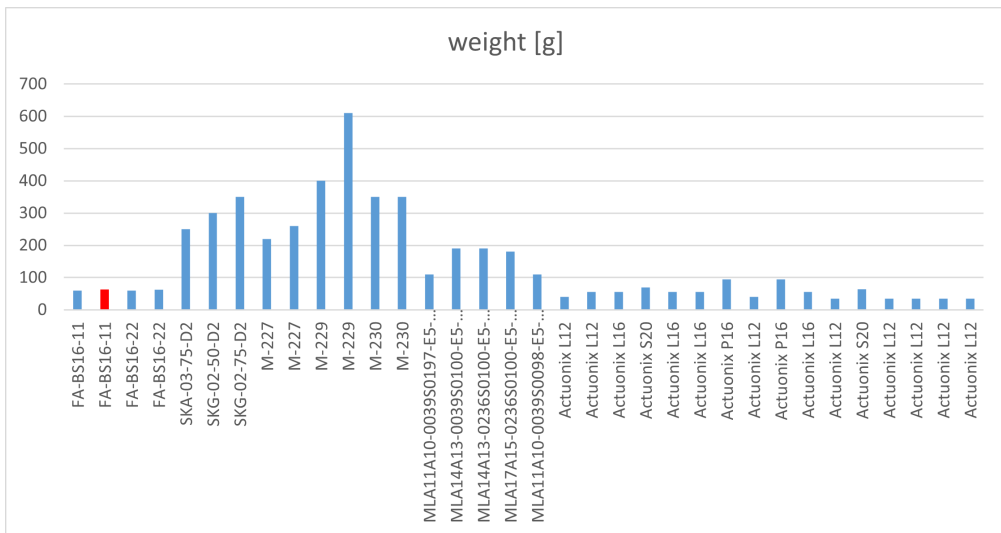
Figure 5.7: Actuators weight comparison.

Chapter 6

CAD parts and structural analysis

The cad realisation and structural analysis are one of the main parts of this thesis, realised since the beginning of the work and modified during the all process to adapt them to the chosen components and the force developed.

During the first phase of the work, not all data were clear and most of them could change multiple times.

For this reason the CAD realization in software shall be realised using a parametric definition of dimensions.

The design of the various parts was performed mostly on Autodesk Inventor, a software developed for mechanical part realisation and which also includes some useful features to perform different kinds of analysis. SOLIDWORKS was also used to read and export some other CAD files.

For the steady structural analysis were used Autodesk Inventor, Nastran (the extension of Inventor Nastran to be precise) and Ansys.

This type of procedure was chosen to compare different analysis results for the same CAD piece since the softwares aviable are limited to the students edition, so the results are approximated in different ways by different softwares: for example the number of points or the mesh elements given by Nastran could be different from the ones given by Ansys.

Additionally the materials are characterised slightly differently from a database to another one.

To ensure the accuracy of the work the analysis are performed and then the worst condition is chosen to be conservative.

6.1   Arm

The arm (6.1) is a simple structure created to connect the hydraulic system with the nest and allow the injection of the liquid.

To be considered the length of the arm for various aspects. First of all, the impact factor between the drone's propellers and leaves and branches of the trees is a crucial factor, the arm shall be long enough to perform its operation at a safe distance for the drone.

The fact that the nests are exposed to the sun, for larvae survival, is advantageous because they are obviously more reachable, but the risk of impact with other objects, from other trees or from debris that fall off branches above the one the drone is operating with or with objects moved by the flow of its propellers, cannot be excluded.

The length of the arm brings with itself a very important factor that must be considered in the analysis: being very elongated it considerably changes the position of the centre of mass shifting it in front of the drone.

To avoid or at least compensate for this, the rest of the structure and equipment shall be distributed in a certain way (for this reason is decided to assemble the tank and the pump in the rear position, making the base itself more heavy and consistent at the end of the drone).

Figure 6.1: Injection arm

After visualising online papers about nests and the other two projects mentioned at the beginning of this document, is assumed that the right length of the tube is about 1.2 metres, but more or less 20 cm of this length (for the design chosen) are located under the drone and not available for the part of the arm in suspension.

Then approximately another 50 cm of length (measured in the final CAD assembly) are occupied by the propellers even if this part is not totally covered.

The size of the boom diameter was chosen on the basis of the commercial rubber or PVC hose to be used for the liquid, which not only had to be compatible with the boom in order to physically pass through it but also, on the basis of its internal diameter, had to be able to fit the upstream pump outlet.

Considering the chosen pump, the supplier recommends a pipe (adaptable in various lengths) of 3.5mm internal diameter and 1mm wall thickness.

Then two possible solutions were compared and analysed based on the material that is possible to use: the aluminium or the carbon fibre.

Both of them are light materials.
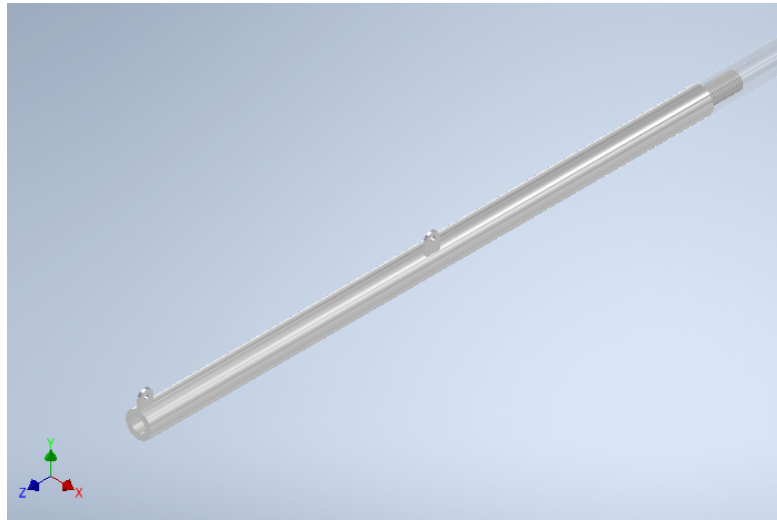
Figure 6.2: First part of the arm
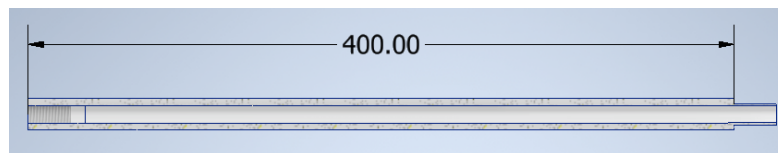
Figure 6.3: Section of the single tube part

For the avant-garde design of this system, after a consultation with the stakeholders, it was decided to opt, at least in a first phase, for aluminium alloy 6060 due to the greater ease of processing in manufacturing companies and thus the possibility of creating joinable pieces instead of monoblocks.

This design idea makes it easier to scale up the system in the event that the length needs to be changed.

The idea behind it is the construction of modular aluminium pieces, each 40 cm long, with a male thread at the front end to be screwed into the next piece, and a

female thread at the rear end to allow the insertion of the previous piece of pipe (detail in the figure 6.3).

Only the first tube, the one that will be in contact with the control system (and thus actuator and base), has two protruding parts on its back that will allow it to be connected by means of two pins allowing freedom of rotational movement. This is shown in the picture 6.2.

The position of the pins is determined according to the calculations made for the application of the force and the position of the arm's rotation pivot.

The pivoting point are important for a d.o.f. point of view represented in the following two pictures (6.4 and 6.5).

This aspect will be discussed also in the actuator paragraph.
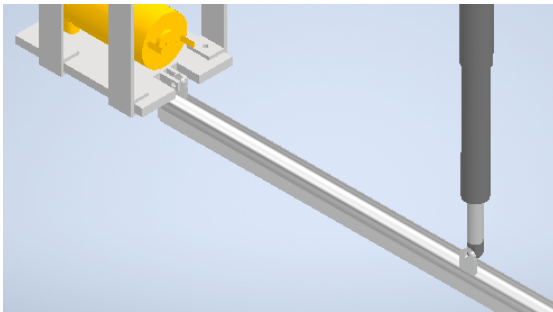
Figure 6.4: Zoom on base-arm assembly.
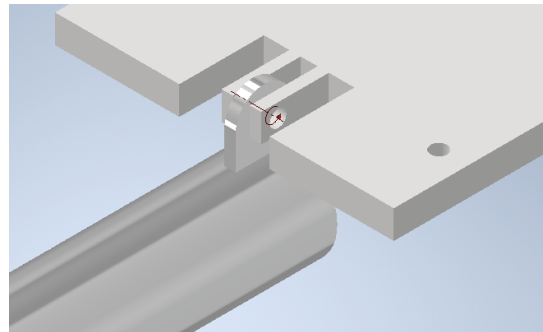
Figure 6.5: D.o.f. arm.

The sizing in external diameter (and therefore wall thickness of the tube) was done considering two aspects:

- the presence on the market of tubes of that size, produced by extrusion and therefore by machinery that has the appropriate outlets for that type of section to be extruded;

- the ability of sections of that size to withstand the operating loads they will be subjected to.

For the first point, an online search was conducted on the primary manufacturers of aluminium tubes, while for the second aspect, were selected the diameters in the market suitable for our applications and performed static structural analyses on Inventor and Ansys software.

Therefore, in order to accommodate the PVC tube and in accordance with the consideration expressed, an inner tube diameter of 10mm and an outer diameter of 20mm are adopted [39].

Another critical factor is the bending of the arm when subjected to forces (including its own weight) that shift its tip position.

Subsequent analysis of this, with the chosen arm length, leads to a small displacement (just 11mm), negligible compared to the size of the nest, which is about the size of a football (28cm).

So there is not significant difficulties and there will be no risk of missing the nest.

In particular, the flexural analysis of the rod was carried out considering the realistic worst case scenario described by the figure 6.6.

By simulating a static analysis with the rod assembled from its three modules, the attachment constraints are defined in the hole intended for connection to the base and, to simulate the condition of a stationary drone in hovering, the surface at the end is fixed on the drone side of the rod.

In this way, an interlocking is simulated.

Regarding applied forces it is described a situation in which gravity is considered.

Additionally were considered a downward force at the tip of the rod of 50N (simulating an additional load of a fairly arbitrary value to be conservative, but representing the situation in which the actuator's ascent is completely counteracted) and a force of 50N in the opposite direction to simulate the operation of the actuator in motion, applied precisely to the hole where the connecting pin between the arm and the actuator will be placed.
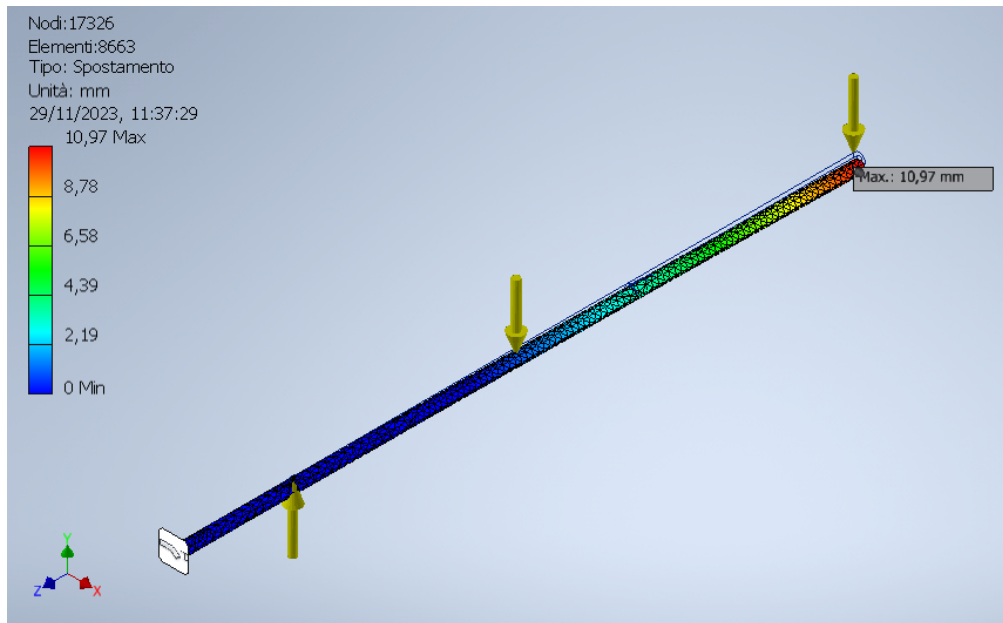
Figure 6.6: Arm worst case

The mesh size was varied from the basic settings to obtain a more reliable result, by densifying the grid and obtaining for this assembly, as can be seen in the data shown in the figure, a number of nodes of 17326 and 8663 triangular type elements that best fit the curves of the pipe.
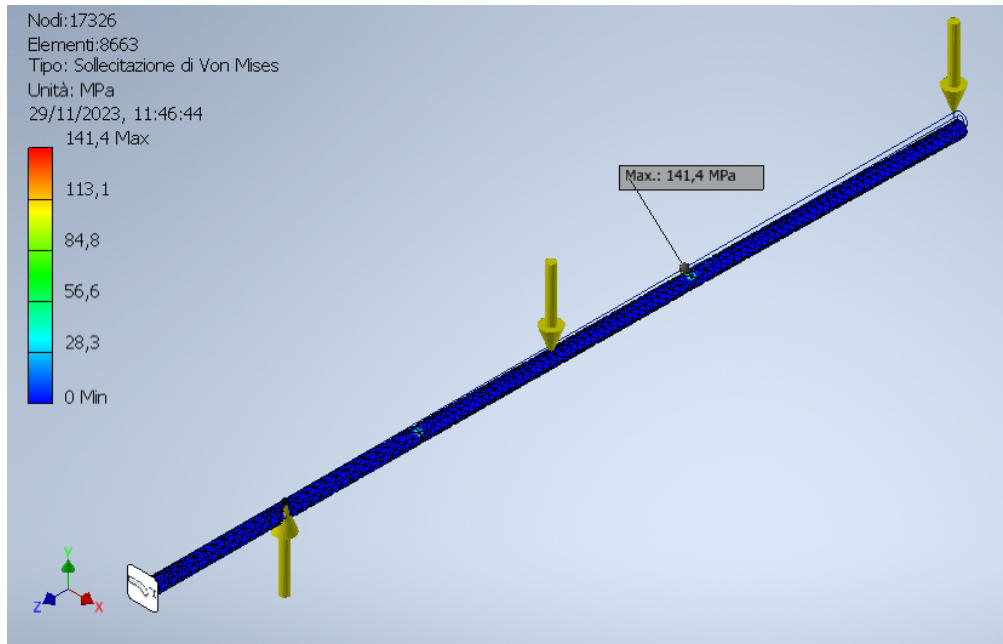
Figure 6.7: Von Mises stress of the arm in the worst case load condition.

Analysing the Von Mises stress, in the worst case scenario, the maximum value is 141.4 MPa at the junction between the second and third pipe sections as seen in figure 6.7.

This datum will then have to be verified in more advanced phases of the project as it is precisely at the thread, which Inventor does not analyse in the most appropriate way because it sees it as an entity but does not consider the exchange of forces between the crests of the threads.

Given this value of stress we will have at this maximum a minimum of the safety factor of 1.94, which is still acceptable if we set ourselves, as is generally done in aeronautics, a lower limit of 1.5 (see figure 6.8).
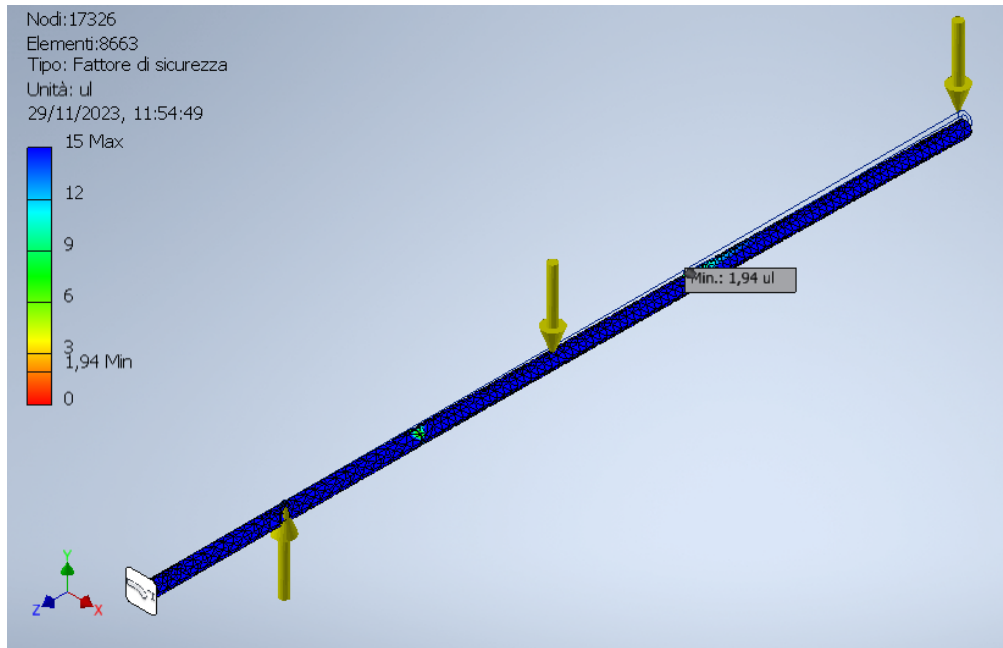
Figure 6.8: Ultimate load factor of the arm in the worst case load condition

For the sake of completeness and a more detailed analysis, some studies are carried out on the first arm section, precisely because it is affected by the greater force exchange due to the presence of the base and actuator attachments.

Going on to carry out an analysis (again with worst condition respect to reality) constraining the end closest to the base and imposing the maximum dynamic force of the actuator (50N) on the appropriate attachment, there is a critical point at the first attachment which reaches a stress of 21.22 MPa shown in the figure 6.9, therefore not particularly worrying.

61
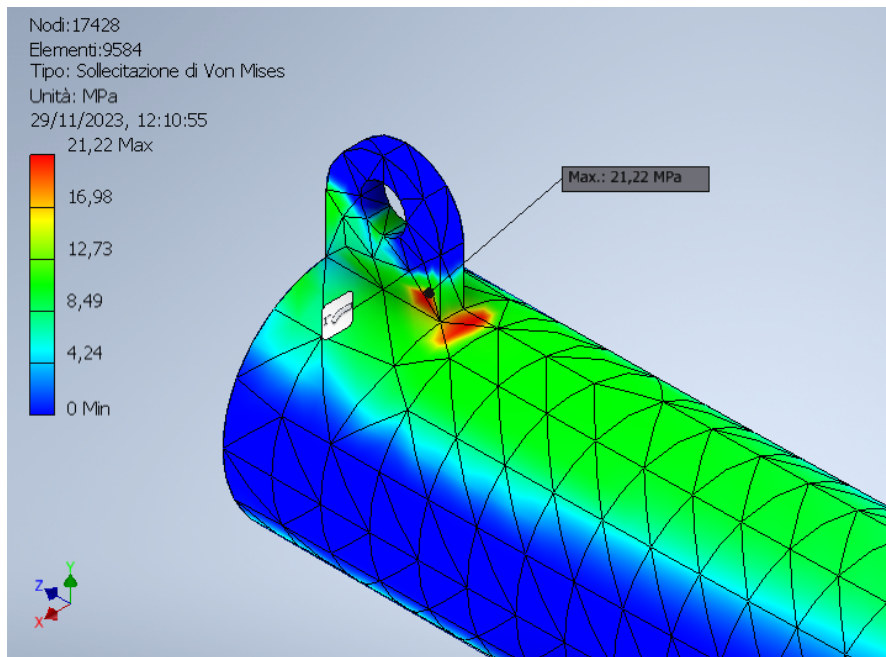
Figure 6.9: Von Mises stress detail on the first attachment

A worrying aspect to check is also the compressive instability of the pipe, given its small cross-section.

Considering the phenomenon of buckling, we know that above a certain critical compressive load, called critical Euler load, in structures such as plates and rods, unstable behaviour occurs with sudden bending in an unpredictable direction.

The critical load beyond which this phenomenon occurs can be calculated using the formula

$$P_{cr} = \frac{\pi^2}{(kL)^2} EI \tag{6.1}$$

from which the critical stress value is derived by dividing by the cross-sectional area.

$$\sigma_{cr} = \frac{\pi^2}{(kL)^2} \frac{EI}{A} \tag{6.2}$$

In the two equations, the terms represent the following physical quantities:

- E is the elastic modulus of the chosen material, expressed in [Pa]. For aluminium E=68.9e9 Pa;

- L is the length of the part being analysed and in this case, wanting to consider the worst-case scenario, we assume that the rod is not constrained at the connection with the actuator but is only constrained at the end, so the total length of the cantilever beam will be 1.2m;

62

- I represents the inertia of the section. For circular sections, the formula is as follows

$$I = \pi \frac{(D^4 - d^4)}{64} \tag{6.3}$$

  where D and d are the outer and inner diameters of the section respectively. In our case the result will be approximately 7.36e-9 m^4;

- A is the cross-sectional area;

- k is a dimensionless number called the effective length factor, which takes on different values depending on the constraint conditions of the rod shown in the table 6.10.

  In the pinned-pinned case, k will assume a value of 1.

  In the fixed-free case, k will be 2.

  For the fixed-fixed case k=0.5 and, finally, for the fixed-pinned case k=0.699.
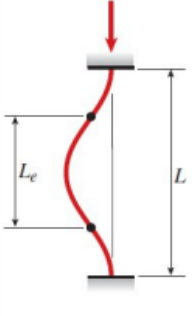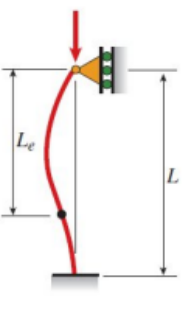
(a) Pinned-pinned column	(b) Fixed-free column	(c) Fixed-fixed column	(d) Fixed-pinned column
$P_{cr} = \frac{\pi^2 EI}{L^2}$	$P_{cr} = \frac{\pi^2 EI}{4L^2}$	$P_{cr} = \frac{4\pi^2 EI}{L^2}$	$P_{cr} = \frac{2.046\,\pi^2 EI}{L^2}$
$L_e = L$	$L_e = 2L$	$L_e = 0.5L$	$L_e = 0.699L$
$K = 1$	$K = 2$	$K = 0.5$	$K = 0.699$

Figure 6.10: Different rods cases and k values [40]

To dimension in the worst case, the fixed-free case (k=2) is represented.

The calculations result in a cross-section inertia of 7.36e-9 m^4 and an overall critical load value of more or less 869N.

Given the forces involved, it can be concluded that the instability of the rod is a negligible phenomenon that has no way of occurring even in the worst-case scenario.

As a matter of fact, as calculated and estimated on Matlab for the force required to penetrate the nest, there will be no need to exceed 5N of force, and the worst cases of more violent collisions in situations of abrupt approach would still be contemplated in loads less than the critical one.
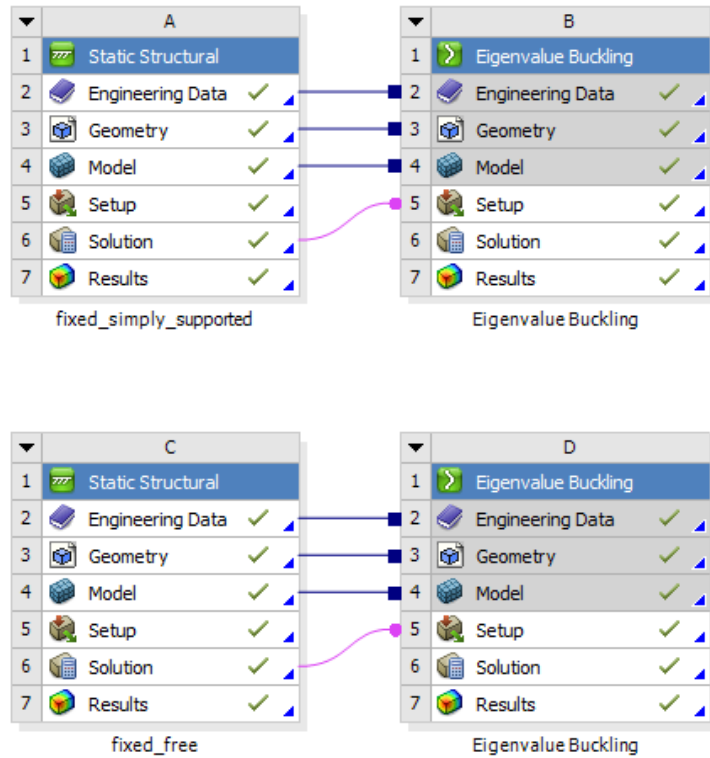
Figure 6.11: Buckling analysis on ansys

The table 6.1 compares the critical compressive buckling load values derived from matlab calculations and the analysis procedure on Ansys (6.11), in the case of a rod with the selected geometry in fixed-simply supported (or fixed-pinned) and fixed-free situation.

6.2   Tank

The choice of tank in this project was partial and needs further consideration. This is not only because the starting point is a design that asks for 10 injections, which

Method	Matlab	Ansys
Fixed-simply supported	7116 N	7055 N
Fixed-free	869 N	900 N

Table 6.1: Critical compression force

in reality could be increased considerably given the wide margin on many aspects (first of all mass and energy consumption), but also because the aim of the thesis is the production of a system with components that already exist on the market where possible.

The difficulty encountered concerns the choice of a tank with a suitable capacity considering also that there may be an initial pre-flight filling phase of the tube running inside the injection arm.

Considering only the presence of the arm of 1.2 metres length, and a pipe cross-section with an internal diameter of 3.5 mm, there is a useful volume equal to at least one injection. Then there is the suction pipe from the tank, the volume of liquid in the pump and another section of pipe joining the pump and arm to be considered.

Furthermore, if the pipe is adapted to the pump inlet but with a larger pipe cross-section, the potential injections contained within the pipe would increase even more.
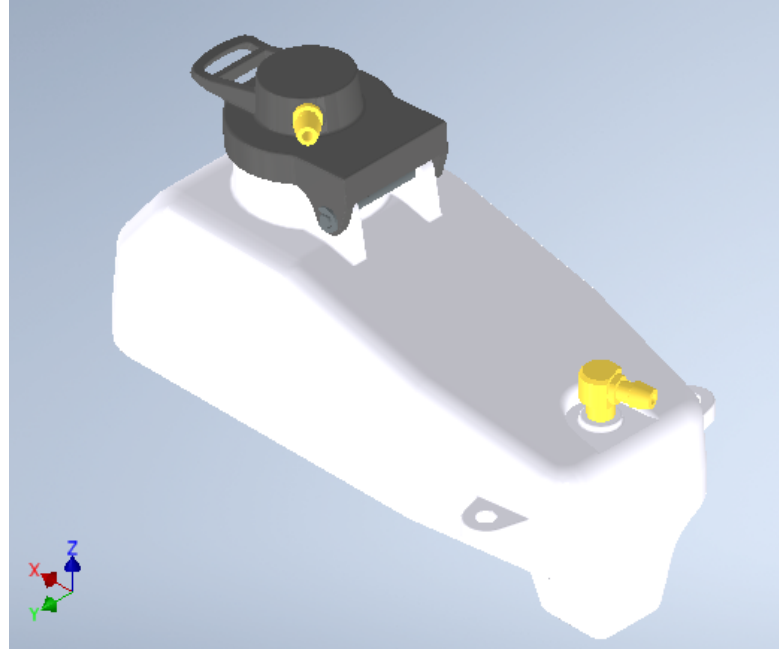
Figure 6.12: Fuel tank of a rc car

65

The other considerable challenge remains the tank capacity, which if it has to be specially chosen on the market from among the agricultural drone tanks, leads to a lower capacity limit of at least 5 litres.

This is precisely because, as discussed in the sections on agricultural drones, the applications are far more substantial and involve spraying plant protection fluid over large areas, of hectares, with large drones.

The solution adopted is the use of a radio-controlled car fuel tank (6.12).

These tanks are usually around 75cc, but there are also many 100cc volume capacity ones.

Furthermore, if one wanted to increase the liquid load, one could also consider putting several tanks in series, and this would not be a problem, but rather an advantage in bringing the centre of gravity towards its starting point.

These considerations will be further explored in the subsequent phases of the project, but for an initial prototype and for the requests made, the single-tank solution is more than sufficient.

The tank was not analysed structurally as it is a pre-built and therefore already tested component. Furthermore, it is neither mechanically stressed by external loads nor internally by pressure loads.

The tank does not require pressurisation of any kind, the work of the pump is more than sufficient for the suction of the liquid and there are no particular changes in altitude that could cause issues.

6.3   Base

The realisation of the base started with the geometric analysis of the drone and the position of different things:

- the position of the screw point that can be used to screw the base to the drone

- the original position of the gimbal and the expected position of the various payloads

- the center of mass

- the need to allocate all the components.

The start point was the CAD analysis of the original DJI gimbal.

This type of attachment is more sophisticated for the necessity of carrying high-performance cameras that have to be controlled in levels of vibrations. It presents a curvilinear form with four total attachment points, two in front of the drone and other two under it. Then there are four dumpers realised in rubber to reduce strong vibrations. Is also important the presence of an input port for the

electrical signal to power the camera and its movement system on three rotational degrees of freedom.

Reducing the complexity of the base, avoiding in the first preliminary design to consider the effects of vibrations, is useful to focus on the dimensioning part of the base: the components.

The architecture of the base can change a lot for various reasons, leading to 10 different prototypes at the end of the work, but the main feature that changes drastically the architecture was the type of leverage we want to introduce.

In the first type of leverage, the actuator shall be placed in the rare position, behind the pivoting point, so all the components in the rare part of the base shall be placed properly and extremely close one to another.

Given the little amount of space to allocate the components this solution is not optimal.

It is essential to have in mind all the considerations and calculations written above on the two configurations.

The third type leverage is more suitable for the drone as it provides a better distribution of weights and components, occupying the available space in a better way.

The most obvious drawback is the slightly forward position of the center of mass since the actuator will be placed at the tip of the drone's body.

However, the mass of the actuator is very small, only 63 grams, and the variation in the center of mass, compared to the advantage of this configuration, is negligible.

After considerating all this aspects, the CAD design is initiate from simple shapes oriented and positioned taking into account the dimensions of the pump and actuator.

For the chosen actuator (as can be seen in the last basic CAD design produced), there is a stroke of 60 mm.

It as to be considered that the space occupancy of the actuator will be the dimension of the case plus half a stroke, i.e. actuator half extended.

This ensures a neutral position providing 30 mm of travel per side, which is what we need according to the calculations made in Matlab.

The only precaution to be taken is that the cylindrical body containing the screw system mechanism does not get in the way of the drone's frontal camera system.

In the realisation of the base, the assembly in terms of degrees of freedom given to the various components cannot be neglected either (see figures 6.13 and 6.14).

Since a rotating arm, mechanically transported by an actuator with an axial movement, must be accommodated, a small amount of rotation must be taken into account in terms of both mobility and overall dimensions, preventing interference between bodies.

Furthermore, due to how the system acts in contact with the nest during the

67

drilling process, there will be forces exchanged that will affect the base, drone and other components such as the arm and the actuator.

These force have to be managed in order to not influence the functioning of the actuator itself.

The actuator, designed for movement with only one degree of freedom, i.e. longitudinal to the extension axis, should not be transversely loaded beyond a certain limit.
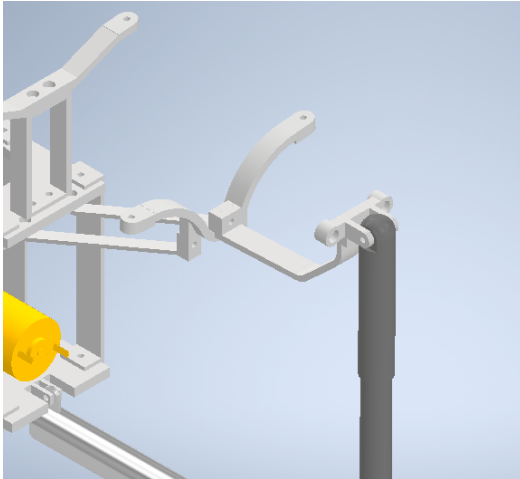
Figure 6.13: Zoom on base-actuator assembly
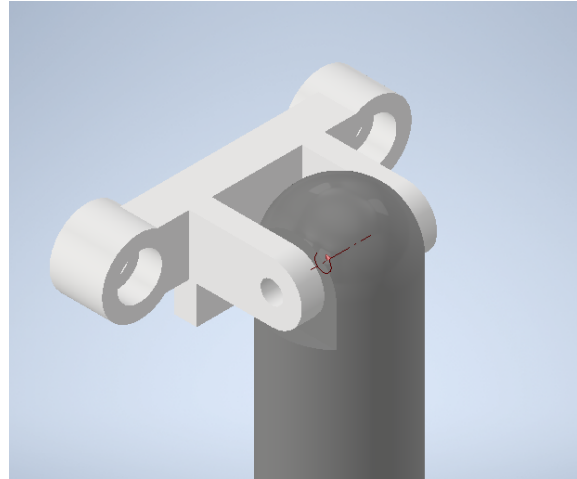
Figure 6.14: D.o.f. actuator

The distance between the pin of the injection rod and the pin attached to the actuator gives us the minimum occupancy of the base (20 cm).

Consequently, now is known where the actuator and pump will be positioned and hopefully, for convenience and to avoid pipe bends resulting in pressure losses, the pump will be placed at the pipe inlet.

This is also to partly balance the position of the centre of gravity with the weight of the pump.

Also the tank, for understandable reasons and similar to those of the pump, is placed at the rear of the base near the pump and tube inlet.

A final CAD of the base can be assembled and is shown in the figure 6.15, while in the figure 6.16 there is an exploded view.

The material for the base can be of various types.

For this purpose, research was carried out into the main materials on the market for 3D printing and the main options are listed below.

It will then be up to subsequent project phases, even after print tests, to choose the most suitable option. The only purpose of this analysis, for now, is to state the
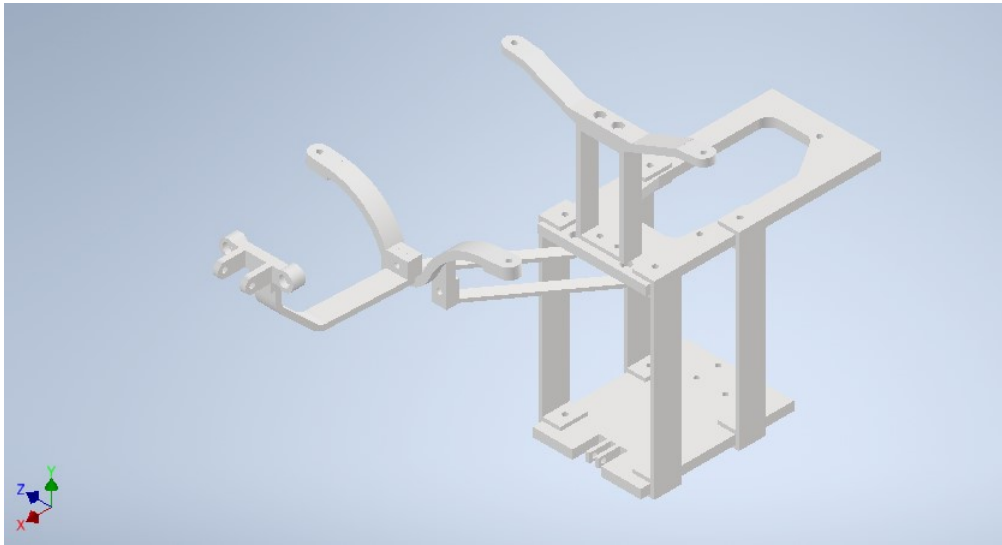
Figure 6.15: Base realised on Autocad Inventor.
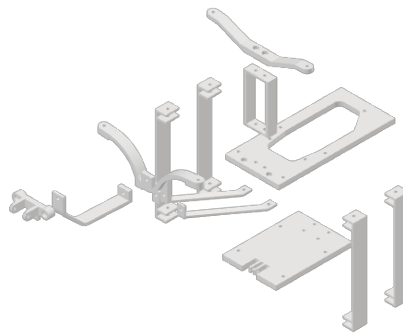
Figure 6.16: Exploded view of the base realised on Autocad Inventor.

feasibility of the choice.

The starting point is an analysis of the most commonly used printing materials, mainly for the sake of printability and cost-effectiveness.

Materials such as PLA and PETG do not require special costs and care, but more innovative materials such as PEEK and ONYX are not only more expensive, but also require a special printing nozzle, making the parts more difficult to produce and more expansive.

In the table 6.2 the most important mechanical property of these materials are resumed.

[41] [42] [43] [44]

feature	density [g/cm^3]	E [GPa]	Tensile strength [MPa]	Softening T [°C]
PLA	1.24	2.35	49.5	60
PETG	1.27	2.02	45	80
PEEK	1.32	3.79	99.9	250
ONYX	1.2	2.4	40	145

Table 6.2: Materials for 3D printing

PETG was chosen as the material for the project because it has the necessary characteristics of strength and lightness combined with low cost and another fundamental aspect, good resistance to thermal softening.

It is clear that there are high-performance materials with much higher characteristics than the choice made, but which involve higher complexity and cost and are sometimes unnecessary for the project's purpose.

Although the price difference with respect to PLA is not substantial, the additional 20°C of thermal resistance can make a difference considering that the electric motors of the components tend to heat up.

The maximum temperature reached by the pump is 80°C [45] , therefore at the limit of the thermal resistance of PETG, but avoiding unnecessary expenses to change material one can simply think of an economical solution such as the interposition of a thin heat-resistant and insulating panel in material such as silicone.

Another option could be distancing the component using vibration mounts.

Once the material has been chosen, the structural analysis of the base proceed with its assembly, defining constraint relationships between the various parts.

To facilitate this phase and to foresee the fastening of the parts, through holes for the various bolts are already prepared.

A solution based on bonding could also be possible, but for now the worst case scenario is handled and also the screws for the connection with the drone are necessary.

Structural discontinuities such as holes will be the site of concentrations of structural stresses to be analysed later.

Taking advantage of the holes enable the use of the coincidence constraint between the various parts with the alignment of the axes of the holes and the contact between the faces.

In addition, it is important to note that the contact parts are designed to reduce the stress on the holes as much as possible distributing it across the contact faces of the various parts.

The yielding for the exchange of forces between different materials (steel and 3D printing material) will be studied again in the next project phase.

Fixing constraints and forces are selected.
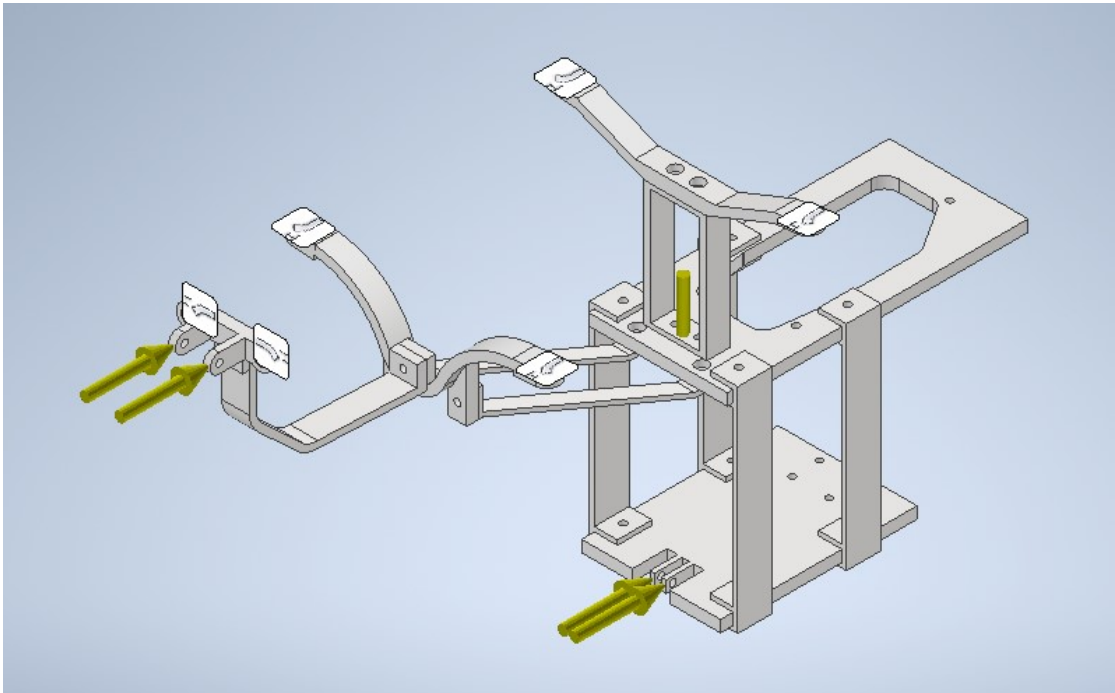
Figure 6.17: Base with constraints and forces applied.

In this case, fixed constraints are located on the faces of the screw holes so that the stress is more equally distributed.

The holes to be fixed are obviously the ones representing the attachment points with the drone.

For the position of the forces, one has to think about the functioning of the system and the way in which operations are carried out mainly during flight.

Knowing, at this point in the design, the positions of actuator and injection arm, it is possible to estimate forces developed and how they are oriented.

In the described operation mode, we will have an almost entirely horizontal interaction with the nest. The maximum value of force inclination will be 5° from the horizontal.

As can be seen from the pictures (6.17) then, the forces (with the exception of the gravitational one) are located in the holes which house the pins.

The forces exchanged with the components will be reflected on the respective metal pins which will exchange these interactions with the hole surfaces.

Is important, as already pointed out, the management of the degrees of freedom of the arm and actuator so that the forces are not a problem for the actuator itself and are distributed in such a way that they do not place transverse burdens on the mechanism.

The force intensity, as seen in the analysis, is very low indeed, just 5N, and distributed, according to the geometry, over 4 different holes.

To make a very conservative analysis then we will assume that these 5N are applied on all four holes, which corresponds to quadrupling the force.
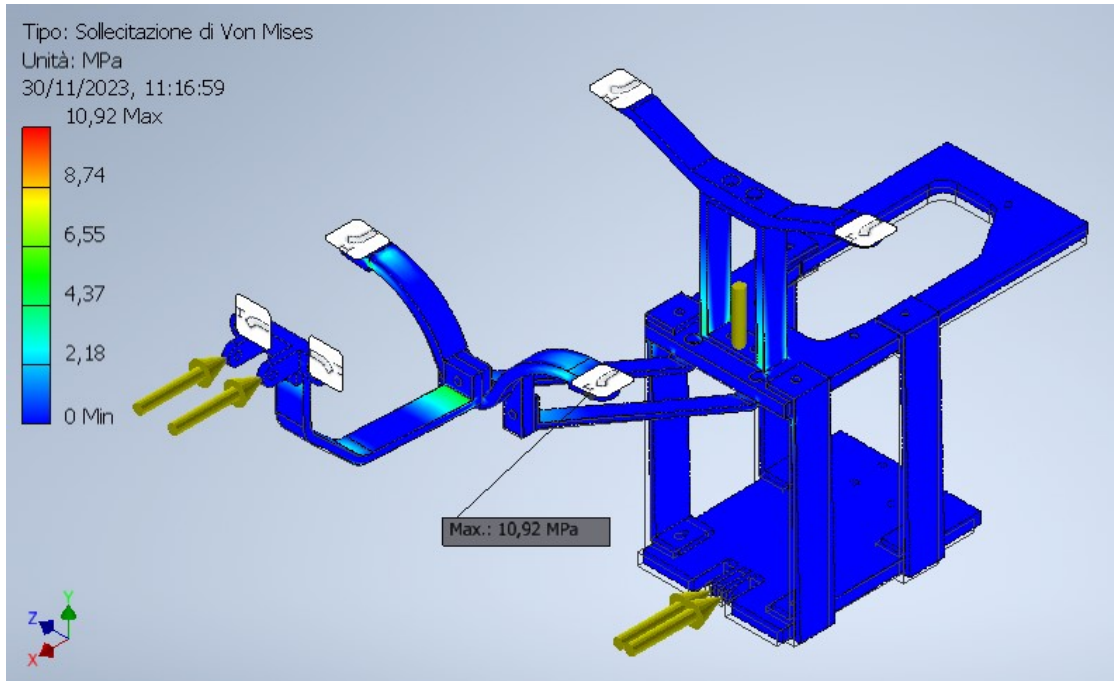
Figure 6.18: Base: Von Mises stress (375282 nodes 234240 elements).

The peak stress value in this case is 10.92MPa (represented in the image 6.18), which gives us a safety factor value of 4.98, thus well above the threshold we set ourselves of 1.5.

The maximum displacement recorded is about 3 mm (represented in the image 6.19), and it can be assumed that it is not significantly reflected in the position of the arm tip.

This deformation, observed at the rear of the base, precisely where major forces (resulting from contact with the object outside the system) are discharged, could be reduced if the system were more compact and did not give way (thanks to the distance from the attachments) to create a momentum around the drone's rear pivots.

However, this solution (adopted by other companies that have already developed a drone system of this type) would not accommodate the actuator and thus the possibility of moving the arm.

Furthermore, the analysis just presented does not foresee the presence of the pump and the tank on these bases, which will have a positive impact by reducing
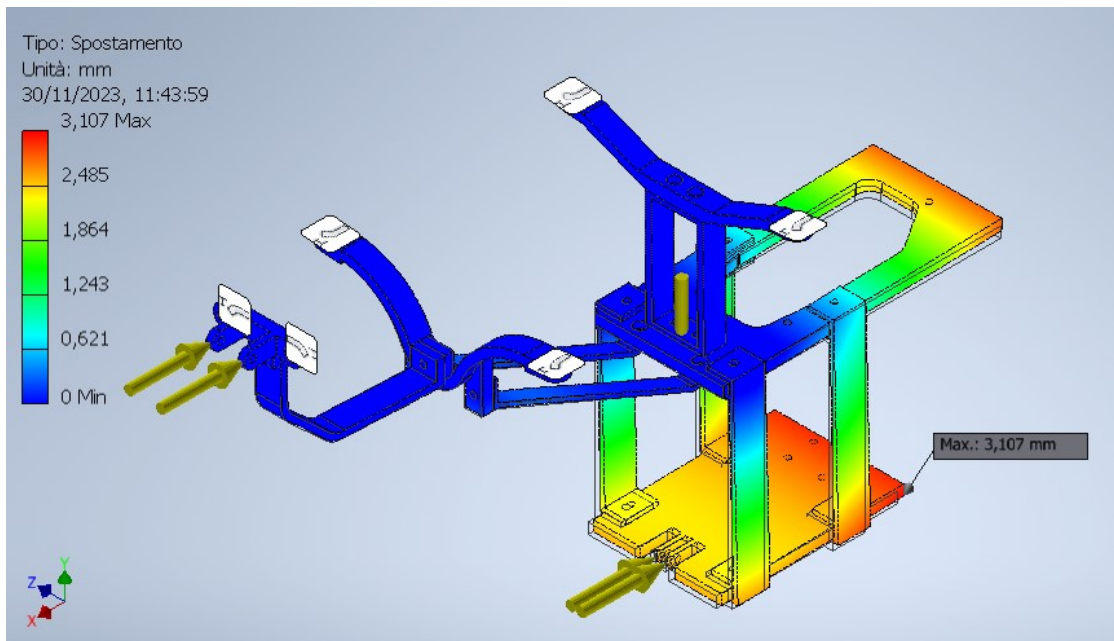
Figure 6.19: Base: displacement (375282 nodes 234240 elements)

deformation as a result of the weighting of the part on which they rest.

On the other hand, there are no significant deformations in the front part of the base as the forces are not discharged in this area due to the rotational mobility of the actuator and they still see a more solid and direct connection with the drone itself.

The same type of analysis is conducted using Ansys for comparison and see if at least, by order of magnitude, the result is reliable.

A premise is necessary: all the software used has student licences with their limitations, or an overly detailed analysis would require too much time and calculation power, so the results depend largely on the accuracy of the mesh created and how dense it is.

For Inventor, meshes with an average element size of 0.02 times the length of the footprint box and a minimum element size of 0.02 times the average size were used.

In Ansys, the mesh is much more limited, with an element size of 3mm as the lower limit for the licence provided and therefore a number of nodes for our part to be analysed of 61980 and a number of elements of 30657.

With these analysis characteristics and imposing the same constraints and forces, we have the results shown in the figure 6.20 and 6.21, which differ slightly from those in Inventor, which, being more critical, will give us more conservative considerations.
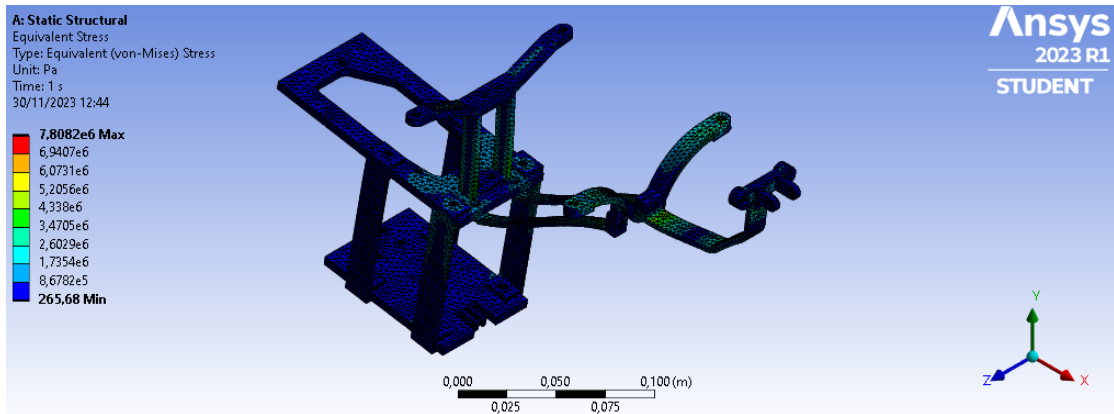
Figure 6.20: Base: Von Mises stress Ansys (61980 nodes 30657 elements)
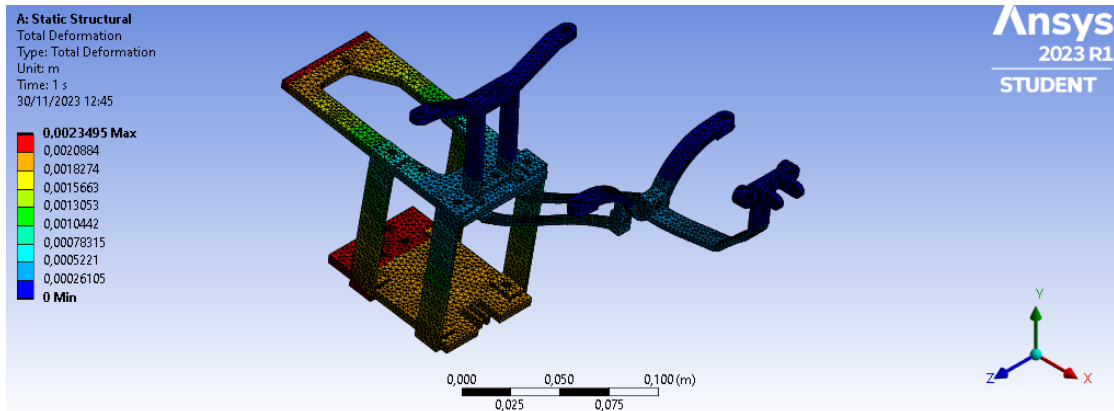
Figure 6.21: Base: displacement Ansys (61980 nodes 30657 elements)

6.4 Other components

For the other components, the CADs were not created but directly provided by the manufacturers on their sites.

They are supplied as almost unique parts and do not include the details of the internal components.

That is why they are only given as a function of their overall dimensions in order to have a system assembly.

Weights and materials are also specified in the respective datasheets but are not really shown on CAD.

For this reason, calculations on the centre of gravity are carried out separately on matlab and sometimes estimated on the basis of the geometry and orientation of the various parts.
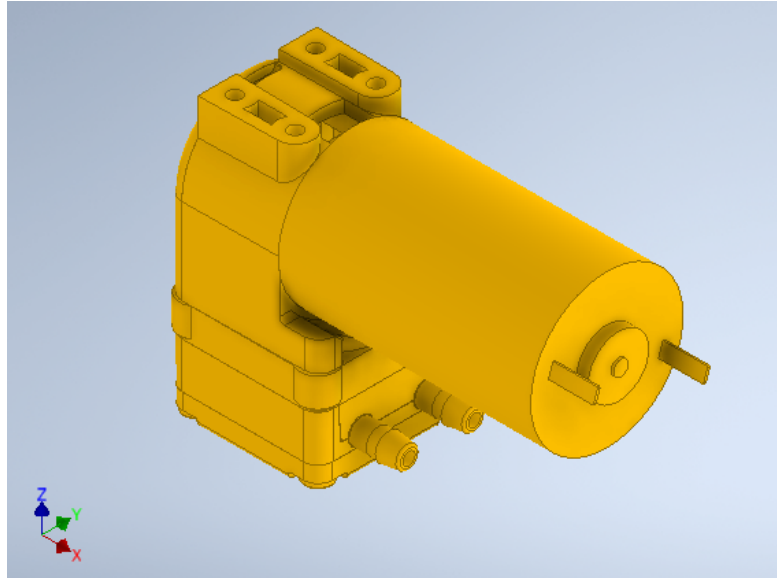
Figure 6.22: Pump 19k from Boxer

On the actuator and the pump we can express a few more characteristics that can be found on the materials site.

The Boxer 19k pump [45] (figure 6.22) has a nitrile diaphragm, silicone valves and EPDM seals, the other liquid-wetted parts are made of PPS (polyphenylene sulphide).

The actuator [38] (figure 6.23), is made of more solid mechanical components and, with the exception of the case, metal: the material of the expansion rod is stainless steel 304 while the external housing material is aluminium T6063.

The complete model (figure 6.24) and assembly with drone (figure 6.25) are shown below.

For completeness, the definitions of the quantities used in the structural analyses are given at the end of this chapter.

The factor of safety is nothing more than a ratio (hence a dimensionless quantity) between the yield stress of the material and the stress measured at a given point on the object studied.

This factor indicates the limit of stress that a component can have and whether this component can withstand certain stresses without suffering irreversible damage: below unity, there will definitely be failure or permanent deformation.

It is therefore advisable to be as far away from this margin as possible.

Von Mises' equivalent stress is instead expressed with the following formula [46],

$$\sigma_v = \sqrt{\frac{(\sigma_{xx} - \sigma_{yy})^2 + (\sigma_{yy} - \sigma_{zz})^2 + (\sigma_{zz} - \sigma_{xx})^2}{2} + 3(\sigma_{xy}^2 + \sigma_{yz}^2 + \sigma_{xz}^2)} \quad (6.4)$$
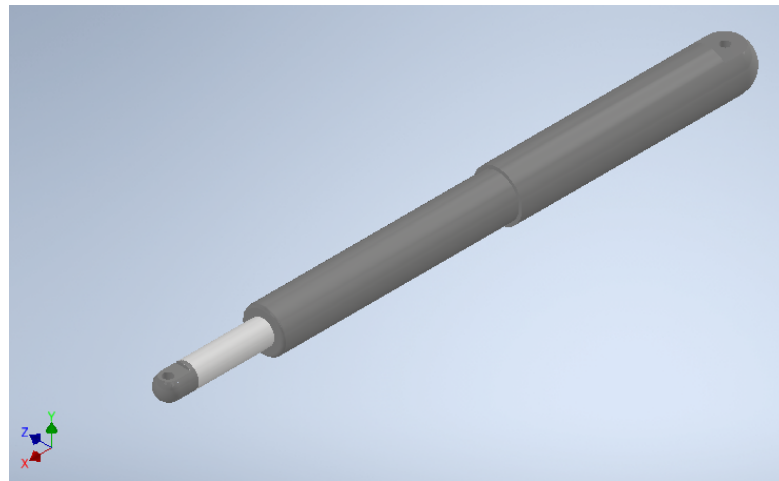
Figure 6.23: Actuator FA-BS16-11 from Frigelli Automations.

Figure 6.24: Assembly.

which combines the stress components of the multidirectional tensor into an equivalent stress.
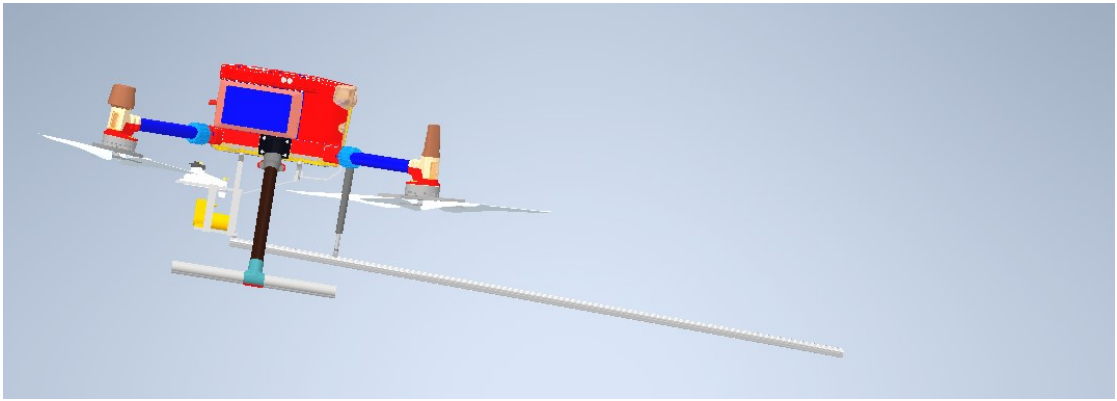
Figure 6.25: Assembly with drone.

This formulation is valid for isotropic materials loaded in the elastic range, where precisely elastic modulus and Poisson's coefficient do not vary for loads in different directions.

Chapter 7

Final analysis and conclusions

7.1 Power and mass budget

The power budget is important to confront the power demand and supply.

It is crucial to understand whether the power consumption of the payload is within the limits of the drone's batteries or whether there will be the need to insert a different battery pack.

This analysis is therefore particularly significant to understand whether it is possible in practice to make savings in weight, complexity and cost.

Taking the drone's autonomy time into account, a timeline can be estimated and then a duty cycle calculated to get an idea of the time the components will be used over the entire operation.

From a first iteration, the components assembled at the base, together with the weight of the liquid, amount to 1.22kg (see table 7.1).

Considering a margin of half a kilo with potential increase in the tank capacity to achieve more injections, all the wiring, electrical boards and various bolts and connections provided, we would still be roughly around a weight of 1.7kg for the payload.

So, based on an initial assessment against the graph given by DJI on flight autonomy 7.1, we can approximate a flight autonomy of about 40 minutes.

Also, the flight autonomy shown in this graph is based on specific payloads and calculated on their power consumption.

These payloads are high performance and high quality cameras, capable of tasks such as land analysis, photogrammetry and thermal analysis.

An example is the Zenmuse L1, which has a power supply of 30W in nominal functioning and a maximum of 60W.

Component	Weight [kg]
Base (PET)	0.091
Actuator	0.063
Pump	0.175
Tank	0.026
Arm (alluminium)	0.768
Liquid	0.100

Table 7.1: Components weight
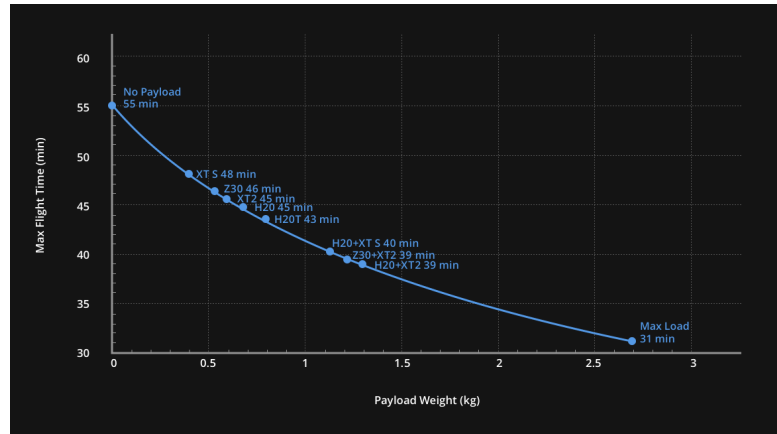
Figure 7.1: Flight autonomy of DJI m300.

In a first approximation, is considered a 40-minute mission based only on the payload in terms of weight and a number of injections equal to 10.

Each injection lasts approximately 30 seconds and includes approaching the nest, penetrating it, injecting the liquid and finally the drone's departure.

Ten injections are performed in an estimated time of just 5 minutes out of the total mission duration.

From here is possible to calculate the duty cycle of the components. This corresponds to

$$DC = \frac{activetime}{totaltime} = \frac{5}{40}[min] \tag{7.1}$$

In order to get an idea of the average power consumed [1], we refer to the calculations obtained from component detailing various consumptions.

In the summary table shown here 7.2, in full then inserted between the appendices, are listed the typical values of power and consumption.

To conclude the analysis, the energy consumption of the components based on the usage time in the various operational phases is determined 7.3.

79

component	Supply voltage [V]	Min load current [A]	Max load Current [A]	Output power [W]	Max output power [W]
Pump	12	0.217	0.8	2.6	9.6
Actuator	12	0.3	0.3	3.6	3.6

Table 7.2: Components power data

The electrical components chosen are only active during the operational phases of injection, while the rest of the time (excluding some possible activation to adjust the pump and arm pitch) they are ideally switched off.

Considering that the pump will be able to keep the liquid in the tube without backflow, due to the presence of non-return valves inside it, there will not be the need to switch it on.

	Nominal phase	Injection phase
Pump	off	on
Actuator	off	on
Total time [s]	/	30

Table 7.3: Power profile on a single injection

Algorithm 1 Power consumption calculation.

1: ▷ Pick power= 13.2W ▷ Given by the sum of the pick power of the different components. Shall be less than the estimated power of the battery.
2: ▷ Energy consumption=0.11 Wh   ▷ This one is representative of one single injection. Given by the product between the pick power and the time of utilization of the system in hours.
3: ▷ Injection number= 10
4: ▷ Total energy consumption= 1.1 Wh   ▷ Given by the product between the number of injections and the energy consumption of a single one.

Finally, there is a comparison between what one has obtained with the nameplate data of the battery 7.4.

Voltage	52.8 V
Capacity	5935 mAh
Energy	274 Wh
Estimated power	298,9 W

Table 7.4: LiPo 12S battery

Considering that there are two batteries on the drone, and comparing the power consumption from the calculation in the algorithm 1, with the power supplied, it can be established that the addition of an external battery can be safely avoided, saving in weight, complexity and cost.

The positive aspect of the addition of the battery would be the retreat of the centre of gravity, which is now about 22cm forward in relation to the nose of the drone, and results in a momentum in relation to the drone's centre of gravity of about 4.5 Nm, which can be fully managed by the propellers.

7.2   Cost analysis

To set a sensed cost analysis, it is necessary to set a budget on the project based on the investors and the income that the operative system, once it is usable or sellable, can provide to the stakeholders and the company who commissioned it.

In this thesis there is only a first part of the project that does not involve all the components (especially the ones related to the control system to be chosen) and the ones involved are taken in consideration only in a first phase project, but they can be changed.

In a project, the impact of changes have different consequences in different stages of the life sequence of the project: during a planning phase, which is at the beginning, the impact of changes is significant, but the cost of changes is relative low.

On the other hand, when the implementation phase is arleady underway, there is a low impact of changes because most of the components have arleady been chosen. However an unexpected change can cause a not negligible cost variation.

For these reasons, performing a cost analysis is premature and limited but it can give an idea about how to proceed and is also necessary for selection of components.

We will limitate the cost analysis only at the cost of the components and the operations, comparing them with the costs of the drones and components appositely designed for agricultural applications and with the traditional methods used for disinfestation of processionary's nests.

Starting a list of costs (resumed in the table 7.5), there are some voices to be mentioned:

- materials cost;

- cost of tools (for example the 3D printer for the base);

- cost of equipment: pump, actuator, tube, arm, needle;

- cost of the drone (battery recharge and eventually cost of damaged component to replace);

- cost of the liquid produced by the scientific community used for the nests;

We can assume that the tools to use for the production of the required pieces are already possessed by the company for which I am working for, so for the voice "tools" we can add the costs for the material to be used in production (for example the wire for the 3D printer assuming that the company arleady possesses the 3D printer).

Product	Market cost	Material cost	Production cost
Pump	125.96 €	/	/
Actuator	127.78 €	/	/
Arm (alluminium alloy)	/	16.35 €/m	/
Base (PET)	/	29.99 €/kg	from 5 to 20 €/h
Inner tube (1 m)	6€	/	/

Table 7.5: Table of costs for the components

Is good practice to estimate benefits: a traditional operation for nest removal can cost about 150/200 € per tree because it is an operation that requires a very careful procedure with technical equipment and trained operators.

So, even if the cost analysis is not complete, we can project it assuming that the cost of the equipment is almost covered in an operation involving a single tree (also we know that in a forest it is very likely that is not a singular tree to be infected).

Then will be added the costs linked to the project, the costs of validation tests and the operator that physically fly the drone (but in a further phase the drone will be autonomous).

There are different ways to perform a cost estimation.

- detailed bottom-up estimating: is the most detailed estimation technique based on the cost of materials and produce cost of each element. Is the method used when all the data are available and at a detailed design phase.

- analogous estimating: is the most indicated for projects that are similar to others existing ones. Is based on a comparative method adjusting the differences for size, mass, material or complexity between two projects. The advantage is that this method can be used at any stage of detail in the system.

- parametric estimating: uses equations called Cost Estimating Relationships (CERs) to calculate prices based on some values like mass, length, material...

In our case we do not have all the parameters and detailed design data to make an accurate cost analysis based on the bottom-up procedure, but on some components the choice was performed, so we are able to give a pice from the producer catalogue.

For the remaining part of the cost analysis will be used an analogy or parametric approach.

Indeed, this programme is not totally new as is stated in the introductory paragraphs, but we do not have acess to data involving costs and components used.

To have an idea and a reference we can take the Fitostinger sl data: the total project has a 71429.00€ cost, and 50000€ were EU contributions [47].

This can be the starting point for our analysis, but we have to take in mind that the purpose of our project is to be cheap and low budjet.

Also there is a difference in the components: we have a movimentation of the arm involved and a different material to use for it.

All the differences between the projects are shown in the table 7.6.

When possible it is necessary to do adjustments as objectively as possible: it is desirable to be able to quantify differences in size, performance, complexity and technology.

Parameter	Fitostinger	Fitobiotech	New system
Drone	/	Specifically designed	DJI m300/350
Pump	Diaphgram	Diaphgram	Diaphgram
Actuator	no	no	Micro acuator

Table 7.6: Analogy cost technique: Fitostinger and Fitobiotech

The differences can be compared also respect to an agricultural drone and that is obviously a lot different from the kind of application carried out by Fitostinger and Fitobiotech, but is a more estabilished sector so is easyer to find data about costs, components and also final products (table 7.7).

Parameter	1	2	This project
Drone	ABZ Innovation L10	DJI agras T30	DJI m300/350
Drone cost	13371 €	16000 €	13600 €
Payload	15.4kg	50.1kg	2.7kg
Tank	10 l	30 l	0.1 l
Pump	Diaphgram $5\frac{l}{min}$	piston pump $4\frac{l}{min}$	Diaphgram $0.8\frac{l}{min}$

Table 7.7: Analogy cost technique: agricultural drones

The analogy method is applicable before knowing details in the program and, if the analogy between the new system and the existing ones is strong, the cost

estimation is reliable.

As shown in the table 7.6, many times is difficult to find detailed cost from other programs and there is a tendency to be too subjective in the analysis.

The bottom up technique is then applied to the lowest level summing the detailed estimation, using also what is called Engineering build-up process, in which the costs of buildings, infrastructures, energy, labour hours are calculated.

In this phase of the project is obviously too soon to apply this kind of approach but some consideration can be done because, as said before, components and material (in a first approximation) has been chosen.

Other reasons for not apply this method are that it is time consuming and not flexible because applied to a specific solution: if we want to consider others alternatives we have to create new estimations for each one.

Then is important to compare the costs based on the operations when the drone will be fully operative.

Is early for us to fully understand how the operations and the operator guiding the procedure (and in the first phase also the drone) will affect the cost.

But we can have all the informations to calculate the cost of a common nest removal based on market data on nowadays most known processes and company.

Considering an economic and environmental study [48] carried out in Portugal on the subject of processionary moth removal in pine forests, the average economic profit of the various companies can be established.

The paper already exposes the social and ecological necessity of undertaking treatments in forests affected by processionary moth infestation, reiterating how this is harmful both to other living species and to the health of the forest itself, which visibly deteriorates under the effect of an excessive infestation of this parasite.

Ecological methods were applied to avoid the spread of pesticides and environmental contamination.

The most popular method to date is the use of a preparation of Bacillus thuringiensis kurstaki, a micro-organism capable of attacking the larva by acting on its nervous system.

The economic analysis method adopted in this research is the Cost Benefit Analysis, but our interest in this research is based on the cost of treatment only.

The reported cost of spreading (usually by helicopter) Bacillus thuringiensis kurstaki is 60€ per hectare.

After all these considerations we stop here with the cost analysis, knowing that it is partial and incomplete.

The operational costs will be established later by the company.

Only for data availability some components have been excluded, but if we wanted a very cheap product we could have selected components that, in some cases, cost less than the 25% of the cost of the component selected.

This method involves a different approach, in which the productor has to buy

components whose specifications are not clear and try them testing all of them separately first in a controlled environment, such a laboratory, and then assembling all the systems on the drone.

In particular for the pump and the actuator there were different alternatives, such as the pumps used in the car to wash the windshield. These kinds of pumps are membrane pumps of 10€ or something more.

At the end of the study, it can be seen that the cost of the system alone amounts to approximately EUR 288 (not taking into account production costs, which are not certain at the moment).

7.3 Environmental aspect

As already mentioned, the method to be adopted with drone injection inside the nest itself is a targeted and very precise approach, selective and non-dispersive from the point of view of the liquid responsible for killing the larvae.

Let us always take as a touchstone the most widespread method, treatment using Bacillus thuringiensis bacteria.

This treatment, although aimed at destroying the larvae and therefore very selective by nature, requires certain important precautions to be taken.

Even in the best case scenario, i.e. the targeted treatment of the nest by means of a backpack sprayer with an operator, spillage into the environment is unavoidable and entails the use of protective clothing and caution in the use of resources (especially foodstuffs) in the treated environment for the deficiency time of the product containing the bacterium, which on average is three days.

The following is a study carried out in Sardinian territory on the long-term effects on the soil after Bacillus Thuringiensis Kurstaki treatments over a period of months [49].

The product used is a commercial insecticide preparation of the bacterium, used as written in the paper over the last 10 years on the territory to protect cork oak forests against the gypsy moth (Lymantria dispar L.).

The study aimed to evaluate the persistence of the bacterium and its toxin in three different territories in Sardinia treated with FORAY 48B, NovoNordisk containing Btk (approx. 10^8 cells ml^{-1}; 12,400 I U mg^{-1}) in May of 1993, 1997 and 1998.

It showed that the bacterium is able to compete with the indigenous microbial community by remaining constant in numbers for 28 months.

Its toxicity also remains, in reduced concentration, for the 28 months post-treatment.

At the end of the study, it was stated that the bacterium and its toxin can persist in the soil for long periods, 88 and 28 months respectively.

As stated by the study "If production exceeds consumption and inactivation by insect larvae, microbial degradation and abiotic inactivation, the toxins could accumulate in the environment to concentrations that may: (1) enhance the control of target pests; (2) constitute a hazard to non-target organisms, such as the soil microbiota, beneficial insects (e.g. pollinators, predators and parasites of insect pests) [...] and other animals; and (3) result in the selection and enrichment of toxin-resistant target insects [...]. Therefore, the potential effects on the environment of this agrotechnology need to be evaluated.".

7.4   Conclusions

In conclusion, from the analyses made from a structural, economic and environmental point of view, the proposed solution is feasible, and this is also proven by the projects already implemented.

In particular, low budget and easily implemented solutions can be adopted to create a system to address a very current environmental problem.

The system is easily realisable with commercially available or similar components, and one can also opt for cheaper solutions regarding the choice of components.

The one chosen in this project were also selected for the sake of data availability, but there are cheaper solutions on the market that will, however, require laboratory testing to compensate for the lack of data provided by the manufacturers.

The base is 3D printable and it will be possible to further optimise it. Moreover, the additive manufacturing technique allows (depending on the filling and printing directions chosen) the structure to be further lightened without losing mechanical performance.

As for the injection arm, a carbon fibre tube was also considered, as briefly outlined in the paper. The reason why the analysis of this solution was not pursued is that for an avant-garde phase such as this, aluminium was opted for due to the easy availability of the product in agreement with the companies involved and its machinability.

This makes it possible to create a modular and machinable solution that does not weaken the composition of the structure, unlike the carbon fibre solution that would have to be taken as a single, bulky tube (even during transport) that cannot be machined if one does not want to weaken it mechanically.

When, at a more advanced stage of the project, more in-depth structural analyses will be carried out on composites, it will be possible to adopt this solution of the prefabricated carbon fibre tube, which certainly has structural advantages over metal alloys and a weight saving that will facilitate a re-centring of the centre of gravity towards the drone.

Another crucial point is the selected drone.

This certainly has, in some cases, a lower cost compared to agricultural-type drones, but at the same time has limited performance (in terms of payload).

The fact that it was already in the stakeholder's possession was the reason for basing the project on this type of drone, and the final result of the thesis shows how the solution is feasible and applicable to this aircraft even if it was not designed for this type of mission.

It will certainly be the task of the subsequent phases to further adapt it to the handling of such a payload, which entails a different flight approach per type of operation and which will also see a revision of the internal control.

Appendix A

Matlab codes

Attention: the code is in matlab live editor, so the lines aligned to the left are text lines, not code.

A.1   DJI m300

```
1      close all
2      clear
3      clc
4 DJI m300
5 data sheet
6 aircraft
7 dimensions without propellers [mm]
8      DJI300.length=810;
9      DJI300.depth=670;
10     DJI300.height=430;
11     DJI300.diagonal=895;
12 weight [kg]
13     DJI300.maxTOW=9;
14     DJI300.maxpayload=2.7;
15     DJI300.OEW=DJI300.maxTOW-DJI300.maxpayload; %
    operative empty weight
16 hovering accuracy
17     DJI300.verticalaccuracy=0.1e-3; %[mm] with RTK
    enabled
18     DJI300.horizontalaccuracy=0.1e-3; %[mm] with RTK
    enabled
```

```
19  speed (in S-mode) [m/s]
20      DJI300.ascentspeed=6;
21      DJI300.descentspeed=5;
22      DJI300.speed=23;
23      DJI300.maxwindspeed=15; %max wind resistance
24      DJI300.pitchangularspeed=300; %[deg/s]
25      DJI300.yawangularspeed=100; %[deg/s]
26  pitch angle [deg]
27      DJI300.maxpitch=30;
28  time [s]
29      DJI300.maxflighttime=55*60;
30  max service ceiling [m] TOF<=7kg
31      DJI300.maxceiling2110prop=5000;
32      DJI300.maxceiling2195prop=7000;
33  temperature [C]
34      DJI300.mintemperature=-20;
35      DJI300.maxtemperature=50;
36  battery
37  batteries: TB60
38      TB60.weight=1.35; %[kg]
39      TB60.maxnumber=2;
40      TB60.capacity=5935; %[mAh]
41      TB60.voltage=52.8; %[V]
42      TB60.energy=274; %[Wh]
43      TB60.mintemperature=-20; %[C]
44      TB60.maxtemperature=50; %[C]
45  Drone performance
46  Flight autonomy-payload, data taken by DJI website
47      payload_weight=[0 0.4 0.53 0.59 0.65 0.8 1.1 1.2 1.3
        2.7];
48      timeflight=[55 48 46 45 45 43 40 39 39 31];
49      x=0:0.1:3;
50      p=polyfit(payload_weight,timeflight,2);
51      z=polyval(p,x);
52      plot(x,z)
53      grid MINOR
54  Forward thrust-pitch P_mode
55      air_density=1.225; %[kg/m^3]
56      %drone measures (approximated from the CAD)
57      b=0.134; %[m]
58      l=0.261;
```

```matlab
59   h=0.160;
60   area_arm = 4*0.3*0.025 ; %m^2, area of the arms over
     the propeller
61   cd_arm = 4/3; % drag coefficient of the arms (source
     : gasdinamica lessons, cylinder drag)
62   cd_square=1.05; %front face of the drone
63
64   dji_weight=(6.3+[0:0.5:2.5])*9.81; %[N] from 0
     payload to almost maximum takeoff weight
65
66   figure()
67   hold all
68   grid MINOR
69
70
71   for i=1:length(dji_weight)
72       drone_weight=dji_weight(i); %[N]
73       pitch_angle=0:0.1:30; %degrees of pitch angle,
     the maximum of the dji m300 is 30deg
74       speed=0:17/(length(pitch_angle)-1):17; %[m/s]
75       T_singlerotor=drone_weight./(4*cos(deg2rad(
     pitch_angle)));
76       armdrag=cd_arm*area_arm/2*0.5*air_density*speed
     .^2; %Drag created by the arms
77       horizontal_T=4*T_singlerotor.*sin(deg2rad(
     pitch_angle))-armdrag.*sin(deg2rad(pitch_angle));
78
79       figure(1)
80       plot(pitch_angle,horizontal_T)
81       title("horizontal thrust vs pitch angle")
82       xlabel("pitch angle [deg]")
83       ylabel("horizontal thrust [N]")
84       grid MINOR
85       hold on
86       legend(num2str(dji_weight))
87
88       S=h*b*sin(pi/2-deg2rad(pitch_angle))+l*b*sin(
     deg2rad(pitch_angle));
89       Cd=1.05:(0.8-1.05)/(length(pitch_angle)-1):0.8;
90       Drag=0.5*air_density.*speed.^2.*S.*Cd;
91       total_lateral_T=horizontal_T-Drag;
```

```matlab
 92
 93         figure(2)
 94         plot(pitch_angle,total_lateral_T)
 95         title("lateral force vs pitch angle")
 96         xlabel("pitch angle [deg]")
 97         ylabel("lateral force [N]")
 98         grid MINOR
 99         hold on
100         legend(num2str(dji_weight))
101     end
102 In this approximated calculation, the graph shows a
        slowly decreasing trend due to the losses in drag
        that have to be compensated to mantain the drone at a
         constant altitude.
103
104 To have an idea of the force that the drone is able to
        front we can calculate the force of the maximum wind
        speed withstandable.
105     front_area=b*h+0.5*area_arm; %[m^2]
106     wind_force=0.5*DJI300.maxwindspeed^2*air_density
        *(0.5*area_arm*cd_arm+b*h*cd_square); %[N]
107 Center of gravity
108 considering the front gimbal screw as the 0 point (
        origin)
109     pump_weight=0.175; %[kg]
110     arm_weight=0.767743;
111     base_weight=0.0911313; %material: PET
112     actuator_weight=0.063;
113     tank_weight=0.026; %approximated
114
115     liquid_weight=0.1; %100ml=0.1kg
116
117     total_payload_mass=pump_weight+arm_weight+
        base_weight+actuator_weight+tank_weight+liquid_weight
        ;
118
119
120     %[mm] from the first two screws of the base, on the
        front face of the drone
121     z_pump=-230;
122     z_arm=414.11;
```

```
123    z_base = -196.3;
124    z_actuator =18;
125    z_tank = -275;
126    z_liquid = -250;
127
128    z_com =(z_pump * pump_weight + z_arm * arm_weight + z_base *
       base_weight + z_actuator * actuator_weight + z_tank *
       tank_weight)/(pump_weight + arm_weight + base_weight +
       actuator_weight + tank_weight);
129    z_com_liquid =(z_pump * pump_weight + z_arm * arm_weight +
       z_base * base_weight + z_actuator * actuator_weight + z_tank *
       tank_weight + z_liquid * liquid_weight)/(pump_weight +
       arm_weight + base_weight + actuator_weight + tank_weight +
       liquid_weight);
```

A.2   Pump

```
1      close all
2      clear
3      clc
4  Electro-hydraulic pump
5  Data
6  aircraft requirements
7  injection
8      volume_singleinjection=8e-3:0.5e-3:12e-3; %[l]
9      number_injections=10; %number of injections for each
       flight
10     total_volume=number_injections*
    volume_singleinjection; %[l]
11     outside_pressure=101325; %[Pa] the value at sea
    level 101325 must be decreased because proccessionary
    moths are also found in pine forests in the mountains
     between 1000 and 2000m altitude, where the
    atmospheric pressure is lower and can cause problems
    for the NPSH
12     injection_time=4; %[s] first attempt value, time
    from needle insertion to needle extraction
13 fluid characteristics
14     density=997; %[kg/m^3]
15     dynamic_viscosity=1.002e-3; %[kg/(ms)]
16     mass_singleinjection=density*volume_singleinjection
    /1000; %[kg]
17     volume_singleinjectionIS=mass_singleinjection/
    density; %[m^3]
18     flow_singleinjection=volume_singleinjectionIS/
    injection_time; %[m^3/s]
19 liquid line characteristics
20 first attempt diameters
21     tube_diameter=3.5e-3; %[m]
22     tube_length=2; %[m]
23     volume_inside_tube=(tube_diameter/2)^2*pi*
    tube_length*1000; %[l]
24     needle_diameter=1e-3; %[m]
25     needle_length=0.05; %[m]
```

```matlab
26     roughness=0.00002; %[m] from tabular data
     considering PVC tubes
27     Stube=(tube_diameter*0.5)^2*pi;
28     Sneedle=(needle_diameter*0.5)^2*pi;
29     tube_velocity=flow_singleinjection/Stube %[m/s]
30     %u_mean=flow_singleinjection/(pi*(tube_diameter/2)
     ^2);   same equation
31     needle_velocity=flow_singleinjection/Sneedle %[m/s]
32     inside_pressure=(outside_pressure+0.5*density*
     needle_velocity.^2)-(0.5*density*tube_velocity.^2); %
     [Pa] pressure before the needle calcolated with
     Bernulli's equation
33     inside_pressurebar=inside_pressure*1e-5 %[bar]
34 distributed losses in the tube
35     Re_tube=density*tube_velocity*tube_diameter/
     dynamic_viscosity;
36     Re_needle=density*needle_velocity*needle_diameter/
     dynamic_viscosity;
37 laminar flow (the results are right but we consider also
      the roughness to be more precise)
38     tll=8*tube_velocity*tube_length*dynamic_viscosity/(
     tube_diameter*0.5)^2; %[Pa]
39     %same equation and same result
40     tube_laminar_losses=(64./Re_tube)*density*
     tube_length/tube_diameter.*(tube_velocity).^2/2; %[Pa
     ]
41 turbolent flow (Re>2300 and circular section, needle)
     calculating friction factor by oppo calculator and
     then using the formula
42     friction_factor=(0.07*Re_needle.^(-0.13)*
     needle_diameter^(-0.14));
43     needle_turbolent_losses=friction_factor.*density*
     needle_length./needle_diameter.*(needle_velocity.^2)
     /2; %[Pa]
44 needle losses with roughness from Moody diagram
45 roughness_needle=0.046e-3; %[m] from
46     epsilon_D=roughness_needle/needle_diameter; %(
     rugosità relativa)
47     zita=0.09; %friction factor calculated by Oppo site
48     zita1=0.08; %from the moody diagram once Re and
     epsilon_D are known
```

```
49    laminar_loss=density*zita*tube_length/tube_diameter
   *(tube_velocity.^2)/2; %[Pa]
50    needle_turbolent_losses1=density*zita1*needle_length
   /needle_diameter*(needle_velocity.^2)/2; %[Pa]
51 concentrated pressure drop
52    beta_tube2needle=0.5; %needle tube shrinkage
53    local_losses=beta_tube2needle*tube_velocity.^2/2*
   density; %[Pa]
54 hydraulic head
55 we consider the pressure in the tank and outside are the
    same because the tank is not pressurized (pa=pb)
56 all the measure are approssimated until i do not choose
   a pump
57    Hb=0.07; %[m]
58    Ha=-0.04; %[m] height from the input of the pump in
   the tank and the pump itself (geodetic height
   difference <0 if pump above draft level)
59    h=0; %[m] distance between input and output inlet of
   the pump
60    Hg=h+Ha+Hb; %[m] geodesic head (geodetic prevalence)
61
62    g=9.81; %[m/s^2]
63    T=20; %[C] temperature of the liquid
64    pv_H2O=6.11*10^(7.5*T/(237.7+T))/1000; %[bar] water
   vapour pressure
65    Y=tube_laminar_losses+needle_turbolent_losses+
   local_losses; % [Pa] pressure drops
66    %in the individual head formulas Y must be converted
    to metres, remembering
67    %that 1bar=10m approx.
68    %must be (pressure on liquid surface in the tank+
   level
69    %geodetic)>NPSHr (pump data)+ pressure drop+vapour
   pressure
70    NPSH=(outside_pressure-pv_H2O*1e5)/(density*g)+Ha-Y
   *1e-4;
71    NPSHr=3; %[m] data sheet value for the pump (to be
   chosen)
72    value1=outside_pressure/10000-Hg; %convert the
   pressure value into metres and consider pump above
   tank level
```

```matlab
73        value2=NPSHr+Y*1e-4+pv_H2O*10; %convert the pressure
         value into metres (for this reason Y is multiplied
        only for 1e-4)
74        Hmax=(outside_pressure-pv_H2O*1e5)/(density*g)-Y*1e
        -4-NPSHr; %maximum suction height
75  pump characteristics
76        EHpump.flow=flow_singleinjection %[m^3/s] volumetric
         flow
77        EHpump.flowlmh=EHpump.flow*60*60; %[m^3/h]
78        EHpump.flowlh=EHpump.flow*60*60*1000; %[l/h]
79        EHpump.flowlmin=EHpump.flow*60000 %[l/min]
80        EHpump.power=EHpump.flow*1000*60.*inside_pressure/(1
        e5)/600; %[kW] includes conversion of flow rate in
        litres/min and pressure in bar
81        EHpump.effectivepower=density*9.8*EHpump.flow*Hg;
82
83        newInside_pressure=inside_pressure+
        tube_laminar_losses+needle_turbolent_losses+
        local_losses;
```

A.3   Actuator

```
 1      close all
 2      clear
 3      clc
 4  Linear actuator system
 5  Data
 6  of the injection-arm
 7      l=0.40; %[m] length of a single part of the arm
 8      arm.length=3*l; %the arm is made of 3 different part
 9      application_point=0:0.01:arm.length/2; %application
        point of the force
10      arm.mass=1; %[kg] from the cad model
11      arm.outdiameter=20e-3; %[m]
12      arm.indiameter=10e-3;
13      arm.section_inertia=pi*(arm.outdiameter^4-arm.
        indiameter^4)/64;
14
15      arm.Ealluminium=68.900e9; %[Pa] elastic modul
        alluminium
16      k=[2 0.699]; %the coefficient 2 is for fixed free
        cantilever, 0.699 for fixed-pinned cantilever
17      arm.Ncr=pi^2*arm.section_inertia*arm.Ealluminium./(k
        .*arm.length).^2; % [N] critic compression force,
        instability limit.
18  of the motor (hp: nut screw motor)
19      motor.displacement=0.03 %[m]half displacement given
        by the motor (given with the actuator selected), the
        other half has to be considered for the opposit pitch
         in the reverse manouver
20      motor.linear_velocity=5.8e-3 %[m/s]
21      motor.attuationtime=motor.displacement/motor.
        linear_velocity; %[s] attuation time to be compared
        with the time of the pitch of the drone
22      motor.force=50 %[N] given with the actuator selected
23  drone
24      maxpitch=30; %[deg]
25      maxpitchvelocity=300; %[deg/s]
```

```
26 the speed of the motor shall be able to equal the pitch
      velocity of the drone
27 Force and momentum equilibrium
28    g=9.81; %[m/s^2]
29    F=g*arm.mass %[N] the force of the actuator shall be
      at least equal to the mass force (we want something
      more to overcome the dynamic loads)
30 third class lever
31    motor.momentum3=motor.force*application_point; %[Nm]
      shall be bigger than the momentum given by the arm
      mass
32    arm.momentum3=arm.length/2*arm.mass*g; %[Nm]
33    motor.angular_velocity3=rad2deg(atan(motor.
      displacement./application_point))/motor.attuationtime
      ; %[deg/s]
34 arm tip (needle)
35    needle_displacement3=sin(atan(motor.displacement./
      application_point))*arm.length; %we could approximate
       motor.displacement/application_point with the sin of
       the angle
36    %needle_displacement3=tan(motor.displacement./
      application_point)*arm.length;
37    needle_angulardisplacement3=rad2deg(atan(
      needle_displacement3/(arm.length)));
38    needle_angularspeed3=needle_angulardisplacement3/
      motor.attuationtime; %is the same, but the linear
      speed of the motor is bigger because the radius is
      greater
39    needle_linearspeed3=needle_displacement3/motor.
      attuationtime; %[m/s]
40 plots
41    min_mom=ones(length(application_point),1)*arm.
      momentum3;
42
43    figure()
44    plot(application_point,min_mom)
45    axis([0 0.6 0 20])
46    hold on
47    plot(application_point,motor.momentum3)
48    grid MINOR
49    legend("min momentum","momentum applied")
```

```matlab
50      xlabel("application point [m]")
51      ylabel("momentum [Nm]")
52
53      figure()
54      plot(application_point,needle_displacement3,
     application_point,needle_linearspeed3)
55      axis([0 0.6 0 1.5])
56      grid MINOR
57      legend("linear displacement [m]","linear speed [m/s
     ]")
58      xlabel("application point [m]")
59
60      figure()
61      plot(application_point, needle_angulardisplacement3,
      application_point, needle_angularspeed3)
62      axis([0 0.6 0 50])
63      grid MINOR
64      legend("angular displacement [deg]","angular speed [
     deg/s]")
65      xlabel("application point [m]")
66  first class lever
67      motor.momentum1=motor.force*application_point; %[Nm]
68      arm.momentum1=(arm.length/2-application_point)*arm.
     mass*g; %[Nm] do not excede application point: if >=
      to armlength/2 this equation has to be changed
69      motor.angular_velocity1=rad2deg(atan(motor.
     displacement./application_point))/motor.attuationtime
     ; %[deg/s]
70  arm tip (needle)
71      needle_displacement1=sin(atan(motor.displacement./
     application_point)).*(arm.length-application_point);
     %we could approximate motor.displacement/
     application_point with the sin of the angle
72      needle_angulardisplacement1=rad2deg(atan(
     needle_displacement1./(arm.length-application_point))
     );
73      needle_angularspeed1=needle_angulardisplacement1/
     motor.attuationtime; %is the same, but the linear
     speed of the motor is bigger because the radius is
     greater
```

```matlab
74     needle_linearspeed1=needle_displacement1/motor.
    attuationtime; %[m/s]
75 plots
76     figure()
77     plot(application_point,arm.momentum1)
78     axis([0 0.6 0 20])
79     hold on
80     plot(application_point,motor.momentum1)
81     grid MINOR
82     legend("weight momentum","momentum applied")
83     xlabel("leverage point [m]")
84     ylabel("momentum [Nm]")
85
86     figure()
87     plot(application_point,needle_displacement1,
    application_point,needle_linearspeed1)
88     axis([0 0.6 0 1.5])
89     grid MINOR
90     legend("linear displacement [m]","linear speed [m/s
    ]")
91     xlabel("leverage point [m]")
92
93     figure()
94     plot(application_point, needle_angulardisplacement1,
    application_point, needle_angularspeed1)
95     axis([0 0.6 0 50])
96     grid MINOR
97     legend("angular displacement [deg]","angular speed [
    deg/s]")
98     xlabel("application point [m]")
```

Appendix B

Power budget

B.1   Power budget

	A	B	C	D	E	F
1	Component	Supply voltage [V]	Min load current [A]	Max load current [A]	Output power [W]	Output power max [W]
2	Pump	12	0,216666667	0,8	2,6	9,6
3	Actuator	12	0,3	0,3	3,6	3,6
4						
5	duty cycle	Injection	Nominal			
6	pump	on	off			
7	actuator	on	off			
8	time [s]	30				
9						
10	Pick power [W]	13,2	shall be less than the estimated power of the battery			
11	Energy consumption [Wh]	0,11				
12	Injections number	10				
13	Total energy consumption [Wh]	1,1				
14						
15	Battery	voltage [V]	Capacity [mAh]	Energy [Wh]	Estimated power[W]	
16	DJI m300 LiPo 12S	52,8	5935	274	298,9090909	
17	DJI m350 Li-ion	44,76	5880	263,2	287,1272727	
18						
19	number of batteries	2				
20	flight time [min]	55				
21	flight time [s]	3300				
22						
23	other payload	name	weight [g]	power [W]	drone flight time [min]	
24		ZENMUSE P1	800	20	45	
25		ZENMUSE H20N	878			
26		ZENMUSE L1	930	60		

Figure B.1: Power budget

Appendix C

Requirements

C.1   Requirements

Identifier	Title	Text	Rationale / Comment	Specification	Type	Verification Methods
PPM-MSN-010	Start date	The project shall be compliant with a launch in DATE	Stakeholder request	Mission	Mission	Review
PPM-MSN-020	Lifetime	The lifetime of the system shall be at least DURATION	Stakeholder request	Mission	Mission	Analysis, Review
PPM-MSN-030	Budget	The system shall be economic and with low budget components	Stakeholder request	Mission	Mission	Review
PPM-MSN-040	Injection	The injection shall be performed inside the nest	Stakeholder request	Mission	Functional	Analysis, Review
PPM-MSN-050	Components	The component shall be, where possible, off the shelf components	Stakeholder request	Mission	Design	Review
PPM-DRN-010	Payload	The drone shall be able to support the payload	Available space, payloa	Drone	Physical	Analysis, Test, Review
PPM-DRN-020	Injections number	The drone shall be able to perform at least 10 injections per flight	Stakeholder request	Drone	Functional	Analysis
PPM-DRN-030	Drone min temperature	The drone shall operate in an environment with a minimum temperature of -20°C	Datasheet of the drone	Drone	Environmental	Review
PPM-DRN-040	Drone max temperature	The drone shall operate in an environment with a maximum temperature of 50°C	Datasheet of the drone	Drone	Environmental	Review
PPM-DRN-050	Payload weight	The total weight of the payload shall be less than 2,7 kg	Datasheet of the drone	Drone	Physical	Analysis, Review, Test
PPM-DRN-060	Center of mass	The alteration of the center of mass shall be compensated by the propellers	To not alterate the stabi	Drone	Physical	Analysis, Test, Review
PPM-DRN-070	Camera visibility	The camera shall not be covered by the structure of the system	Possibility to implement	Drone	Design	Review, Inspection
PPM-PUMP-010	Pump output pressure	The pump shall be able to supply the right pressure to compensate the losses	Necessary pressure to ir	Pump	Functional	Analysis, Test, Review
PPM-PUMP-020	Draught	The supply line shall be able to draw from the tank in each condition	Operational necessity	Pump	Configuration	Inspection, Test
PPM-PUMP-030	Pressure losses	The losses shall not be higher than the pressure capacity of the pump of 2 bar	Calculation	Pump	Functional	Analysis, Test
PPM-PUMP-040	Pump temperature	The operating temperature of the pump shall be under 50°C	Pump temperature load	Pump	Environmental	Review
PPM-PUMP-050	Pump flow	The pump flow shall be at least 0,18 l/min	Calculation based on in	Pump	Functional	Analysis, Test
PPM-PUMP-060	Pump pressure	The pump pressure shall be at least 1.09 bar	Calculation based on pr	Pump	Functional	Analysis, Test
PPM-PUMP-070	Pump voltage	The work voltage of the battery shall be adapted to the pump voltage of 12V	Voltage compatibility	Pump	Interface	Inspection, Review
PPM-PUMP-080	Pump weight	The pump weight, with the other components of the system, shall be less than 2.7kg	Maximum payload weig	Pump	Physical	Analysis, Review, Test

Figure C.1: Requirements 1

	A	B	C	D	E	F	G
28	PPM-STRUCT-010	Arm resistance	The arm shall be able to withstand 10N compression and 20N trasversal force	Structural resistance	Structure	Physical	Analysis, Test
29	PPM-STRUCT-020	Propeller resistance	The propellers shall be able to withstand the impact with leaves and little debris	Structural resistance	Structure	Environmental	Analysis, Test, Review
30	PPM-STRUCT-030	Propeller interference	The propellers shall not interfere with the injection arm	Necessary space for the Structure		Physical	Analysis, Review, Inspection
31	PPM-STRUCT-040	Attach system	The attach system shall maintain the payload attached to the drone	Structural integrity	Structure	Physical	Analysis, Test
32							
33							
34	PPM-ARM-010	Arm lenght	The arm shall be at least 1.2m long	Avoid possible impacts	Arm	Physical	Inspection, Test
35	PPM-ARM-020	Arm inclination	The arm shall be able to compensate the pitch angle of at least +5° and -5°	Mantein the right inclin: Arm		Functional	Review, Test, Inspection
36	PPM-ARM-030	Penetration	The needle shall be able to penetrate the nest	Need to inject the liquid Arm		Functional	Test
37	PPM-ARM-040	Arm material	The material used shall be able to withstand the forces applied and be light	Structural need for the p Arm		Physical	Analysis, Test, Review
38	PPM-ARM-050	Arm weight	The arm weight, with the other components of the system, shall be less than 2,7kg	Maximum payload weig Arm		Physical	Analysis, Review, Test
39	PPM-ARM-060	Needle diameter	The inner needle diameter shall be at least 1mm	Minimum diameter to n(Arm		Physical	Review, Inspection
40	PPM-ARM-070	Alluminium arm	The arm material shall be alluminium (t.b.d.)	Stakeholder request and Arm		Design	Analysis, Test
41	PPM-ARM-080	Arm diameter	The diameter shall be selected between the possible solutions dimension	Extrusion and mechanic Arm		Physical	Analysis, Test, Review
42	PPM-ARM-090	Arm section	The arm shall have a circular section	Calculation on CAD soft Arm		Physical	Analysis, Test, Review
43							
44							
45	PPM-ACT-010	Actuator speed	The actuator speed shall be able to pitch the arm of 5° during the approaching time	Need to have the arm in Actuator		Functional	Analysis, Test, Review
46	PPM-ACT-020	Actuator force	The actuator shall be able to withstand the weight of the arm and the forces applied	Need to be able to move Actuator		Functional	Analysis, Test, Review
47	PPM-ACT-030	Actuator lateral force	The trasversal force shall be controlled with the d.o.f. of the actuator	Actuator load resistance Actuator		Physical	Analysis, Test, Review
48	PPM-ACT-040	Actuator voltage	The work voltage of the battery shall be adapted to the Actuator voltage of 12V	Voltage compatibility	Actuator	Interface	Inspection, Review
49	PPM-ACT-050	Actuator weight	The Actuator weight, with the other components of the system, shall be less than 2,7kg	Maximum payload weig Actuator		Physical	Analysis, Test, Review
50	PPM-ACT-060	Actuator IP	The Actuator Ingress Protection Rating shall be at least IP45	IP of the drone from tech Actuator		Environmental	Review

Figure C.2: Requirements 2

	A	B	C	D	E	F	G
53	PPM-TUBE-010	Tube material	The tube shall be able to withstand pressure and chemical composition of the liquid	Resistence to the chemic Tube		Design	Review, Inspection
54	PPM-TUBE-020	Tube length	The length of the tube shall be at least 1.20m	To avoid interaction wit Tube		Physical	Inspection
55	PPM-TUBE-030	Tube diameter	The inner diameter of the tube shall be 3,5mm	Output diameter of the p Tube		Physical	Review, Inspection
56							
57							
58	PPM-BTT-010	Battery capability	The batteries shall be able to give the required power supply to drone and payload	Battery capability to per Battery		Mission	Analysis, Test, Review
59	PPM-BTT-020	Battery energy supply	The batteries shall be able to supply at least a 1.1 Wh request of energy	Energy consumption fror Battery		Mission	Analysis, Review
60							
61							
62	PPM-LIQ-010	Fluid temperature	The fluid temperature shall be superior to its icing point	Operating temperature k Ingected fluid		Environmental	Review
63	PPM-LIQ-020	Fluid density	The fluid density shall be similar to the wather density	Calculation and pump c Ingected fluid		Physical	Review
64	PPM-LIQ-030	Fluid viscosity	The fluif viscosity shall be similar to the wather viscosity	Calculation and pump c Ingected fluid		Physical	Review
65							
66							
67	PPM-TANK-010	Tank capacity	The tank shall be able to contain at least 100ml of fluid	Stakeholder request	Tank	Physical	Review
68	PPM-TANK-020	Tank material	The tank material shall be PVC (t.b.d.)	Commercial solutions	Tank	Design	Review

Figure C.3: Requirements 3

Bibliography

[1]   G Dissescu, I Ceianu, et al. «Studies on the ecology of the Oak processionary moth, Thaumetopoea processionea.» In: *Studies on the ecology of the Oak processionary moth, Thaumetopoea processionea.* (1968) (cit. on p. 1).

[2]   *Lotta alla processionaria del pino.* Fitobiotech s.r.l. URL: `https://www.fitobiotech.it/#processionaria` (cit. on pp. 1, 3, 11, 13).

[3]   *OAK PROCESSIONARY MOTH.* 205 Rutgers Street, Maplewood, NJ 07040 973-762-5221. URL: `https://www.bartlett.com/resources/insects-and-pests/oak-processionary-moth#:~:text=Oak%20processionary%20moth%20(Thaumetopoea%20processionea,cerris).` (cit. on p. 2).

[4]   *Processionary Pine Caterpillar - what you need to know.* SurviveFrance. URL: `https://www.survivefrance.com/t/processionary-pine-caterpillar-what-you-need-to-know/230` (cit. on p. 4).

[5]   Campoverde Citizens Matter. *The Pine Processionary Caterpillar.* `https://www.pinardecampoverde.com/ppc.html`. Access: November (cit. on p. 4).

[6]   *OAK PROCESSIONARY MOTH OUR SERVICES.* A CUT ABOVE. URL: `https://www.acutabovetrees.co.uk/domestic-services/oak-processionary-moth-removal/opm-services/` (cit. on pp. 4, 11).

[7]   *Patentino drone.* Droneclass. URL: `https://patentino-drone.it/` (cit. on p. 8).

[8]   *ABILITAZIONE EVLOS / BVLOS.* squaDrone. URL: `https://www.squadronefly.it/abilitazione-evlos-bvlos/` (cit. on p. 8).

[9]   Eliteconsulting. URL: `https://www.eliteconsulting.it/` (cit. on p. 10).

[10]   Manuel Gaviño. *How to eliminate the pine processionary: the 6 best methods.* Viveros Gonzales. URL: `https://viverosgonzalez.es/gb/blog/eliminate-pine-processionary-b70.html` (cit. on p. 12).

[11]   *Bacillus thuringiensis Vebi Insetticida biologico 100 g Pfnpe.* SHERENA SRL. URL: `https://www.perfarelalbero.it/insetticidi-lumachicidi-orto-giardino-libera-vendita/2211-bacillus-thuringiensis-vebi-insetticida-biologico-100-ml-pfnpe.html` (cit. on p. 12).

[12] Fabian Christopher Sasse. «Drone based control of pine processionary moth outbreaks in Mediterranean woodlands.» MA thesis. Universitat Politecnica de Catalunya, 2018 (cit. on p. 13).

[13] *The processionary of the pine.* Fitostinger. URL: https://www.fitostinger.com/en/pest-control-with-drone-technology/pine-processionary/ (cit. on pp. 13, 14).

[14] Wikipedia. *Unmanned aerial vehicle.* https://en.wikipedia.org/wiki/Unmanned_aerial_vehicle (cit. on p. 15).

[15] Matteo Pantalone. «Modellazione e simulazione di un quadricottero multi-rotore». PhD thesis. URL: http://amslaurea.unibo.it/9038/ (cit. on p. 17).

[16] UE. «regolamento Delegato (UE) 2019/945, 12 marzo 2019». In: *Gazzetta Europea* () (cit. on p. 17).

[17] UE. «regolamento Esecutivo (UE) 2019/947, 24 maggio 2019». In: *Gazzetta Europea* () (cit. on p. 17).

[18] ENAC. «regolamento UAS-IT edizione 1, 12 marzo 2019». In: () (cit. on p. 17).

[19] *Categoria specifica (Specific category).* ENAC. URL: https://www.enac.gov.it/sicurezza-aerea/droni/categoria-specifica-specific-category (cit. on p. 18).

[20] *Regulations.* EASA. URL: https://www.easa.europa.eu/en/regulations (cit. on p. 19).

[21] *DJI m300.* DJI. URL: https://enterprise.dji.com/it/matrice-300 (cit. on pp. 19, 20).

[22] *Tabella grado di protezione IP.* Studio Petrillo. URL: https://www.studiopetrillo.com/files/Tabella_grado%20di_protezione_IP.pdf (cit. on p. 20).

[23] *DJI M300 vs DJI M350 | What's the difference?* Hammer missions. URL: https://www.hammermissions.com/post/dji-m300-vs-dji-m350#:~:text=DJI%20M300%20%2F%20M350%20Use%20Cases,other%20drones%20are%20unable%20to. (cit. on p. 22).

[24] *What are peristaltic pumps and how do they work?* Debem. URL: https://www.debem.com/en/what-are-peristaltic-pumps-and-how-do-they-work/ (cit. on pp. 32, 33).

[25] *How to use a peristaltic pump?* Debem. URL: https://www.debem.com/en/operation-peristaltic-pumps/ (cit. on p. 33).

[26] *How Do Peristaltic Pumps Work?* Albinpump. URL: `https://www.albinpum p.com/en-gb/news/how-peristaltic-pumps-work` (cit. on p. 33).

[27] *PERISTALTIC PUMPS: FUNCTIONING, APPLICATIONS AND ADVAN-TAGES*. Fluid-o-Tech. URL: `https://www.fluidotech.it/en/technical-support/technical-insights/peristaltic-pumps/` (cit. on p. 34).

[28] *How does a diaphragm pump work?* Debem. URL: `https://www.debem.com/ en/operation-diaphragm-pumps/` (cit. on pp. 34, 38).

[29] *COMPONENTS OF A DIAPHRAGM PUMP*. Comet. URL: `https://blog. comet-spa.com/diaphragm-pumps/components` (cit. on pp. 34, 36).

[30] *Air Operated Double Diaphragm Pumps Guide*. North ridge pumps. URL: `https://www.northridgepumps.com/article-211_air-operated-doubl e-diaphragm-pumps` (cit. on p. 35).

[31] *Diaphragm Pumps*. Verder Liquids. URL: `https://www.verderliquids.com/ int/en/technologies/how-are-diaphragm-pumps-used` (cit. on p. 37).

[32] Dr Tushar Chokshi. *Unknown facts about IV cannulation*. URL: `https://www. slideshare.net/drtusharchokshi/unknown-facts-about-iv-cannulat ion` (cit. on p. 40).

[33] *Needle Gauge Chart*. Hamilton. URL: `https://www.hamiltoncompany.com/ laboratory-products/needles-knowledge/needle-gauge-chart` (cit. on p. 40).

[34] *Perdite di carico nelle condotte*. Edutecnica. URL: `https://www.edutecnica. it/macchine/carico/carico.htm` (cit. on p. 42).

[35] Clara PATINI. *Le perdite di carico*. URL: `http://pcfarina.eng.unipr.it/ dispense99/patini119156/patini119156.htm#%3A~%3Atext%3DPERDITE% 20DI%20CARICO%20CONCENTRATE%2C-Le%20perdite%20di%26text%3DEsist ono%20infatti%20anche%20le%20perdite%2Cscorre%20all%27interno% 20del%20tubo.` (cit. on p. 42).

[36] *Guida al fattore Prevalenza Pompa*. Debem. URL: `https://www.debem.com/ it/calcolo-della-prevalenza/` (cit. on p. 43).

[37] Meyer CH et al. «Geometry, penetration force, and cutting profile of different 23 gauge trocars systems for pars plana vitrectomy.» In: *Retina.* () (cit. on p. 48).

[38] *Attuatore di micro penna con feedback*. Frigelli Automations. URL: `https: //www.firgelliauto.com/it/products/micro-actuators?variant= 39553061945415` (cit. on pp. 49, 75).

[39] *ESTRUSI E LAMINATI IN LEGHE DI ALLUMINIO*. Alluminio di qualità. URL: `https://www.alluminiodiqualita.it/wp-content/uploads/2014/ 12/catalogo_alq_web_indnav_-_riquadrato.pdf` (cit. on p. 58).

[40] *Instabilità (Buckling)*. Università degli studi di Roma Tor Vergata. URL: https://didattica.uniroma2.it/files/scarica/insegnamento/174644 -Fondamenti-Di-Progettazione-Meccanica/49799-13-Instabilit_V1-9 (cit. on p. 63).

[41] *Scheda tecnica materiali compositi*. Markforged. URL: https://s3.amaz onaws.com/mf.product.doc.images/Datasheets/Translations/IT/ Markforged_CompositesV5.1_it.pdf (cit. on p. 69).

[42] *Data sheet industrial PEEK*. Xometry. URL: https://xometry.eu/wp- content/uploads/2021/03/PEEK.pdf (cit. on p. 69).

[43] *Data sheet PETG*. Xometry. URL: https://xometry.eu/wp-content/ uploads/2021/03/PETG.pdf (cit. on p. 69).

[44] *Data sheet PLA*. Xometry. URL: https://xometry.eu/wp-content/upload s/2021/03/PLA.pdf (cit. on p. 69).

[45] https://www.boxerpumps.com/diaphragm-pumps-for-liquid/19k/ (cit. on pp. 70, 75).

[46] *Sollecitazione (equivalente) di von Mises*. Autodesk. URL: https://help. autodesk.com/view/fusion360/ITA/?guid=VON-MISES-STRESS-EQ- CONCEPT (cit. on p. 75).

[47] *Fitostinger: pest control drone*. Cordis. URL: https://cordis.europa.eu/ article/id/418469-drone-based-pest-control-system-protects- europe-s-trees (cit. on p. 83).

[48] Paola Gatto, Alessia Zocca, Andrea Battisti, Maria Joao Barrento, Manuela Branco, and Maria Rosa Paiva. «Economic assessment of managing processionary moth in pine forests: A case-study in Portugal». In: *Journal of environmental management* 90.2 (2009), pp. 683–691 (cit. on p. 84).

[49] Cristina Vettori, Donatella Paffetti, Deepak Saxena, Guenther Stotzky, and Raffaello Giannini. «Persistence of toxins and cells of Bacillus thuringiensis subsp. Kurstaki introduced in sprays to Sardinia soils». In: *Soil Biology and Biochemistry* 35.12 (2003), pp. 1635–1642 (cit. on p. 85).